JOURNAL OF GEOPHYSICAL RESEARCH, VOL. 112, A10102, doi:10.1029/2007JA012321, 2007

Correction published 29 December 2007

Solar and interplanetary sources of major geomagnetic storms ($Dst \leq -100$ nT) during 1996–2005

J. Zhang,[1] I. G. Richardson,[2,3] D. F. Webb,[4] N. Gopalswamy,[2] E. Huttunen,[5] J. C. Kasper,[6] N. V. Nitta,[7] W. Poomvises,[1] B. J. Thompson,[2] C.-C. Wu,[2,8] S. Yashiro,[2,9] and A. N. Zhukov[10,11]

Received 6 February 2007; revised 2 April 2007; accepted 25 April 2007; published 12 October 2007.

[1] We present the results of an investigation of the sequence of events from the Sun to the Earth that ultimately led to the 88 major geomagnetic storms (defined by minimum $Dst \leq -100$ nT) that occurred during 1996–2005. The results are achieved through cooperative efforts that originated at the Living with a Star (LWS) Coordinated Data-Analysis Workshop (CDAW) held at George Mason University in March 2005. On the basis of careful examination of the complete array of solar and in situ solar wind observations, we have identified and characterized, for each major geomagnetic storm, the overall solar-interplanetary (solar-IP) source type, the time, velocity, and angular width of the source coronal mass ejection (CME), the type and heliographic location of the solar source region, the structure of the transient solar wind flow with the storm-driving component specified, the arrival time of shock/disturbance, and the start and ending times of the corresponding IP CME (ICME). The storm-driving component, which possesses a prolonged and enhanced southward magnetic field (B_s), may be an ICME, the sheath of shocked plasma (SH) upstream of an ICME, a corotating interaction region (CIR), or a combination of these structures. We classify the Solar-IP sources into three broad types: (1) S-type, in which the storm is associated with a single ICME and a single CME at the Sun; (2) M-type, in which the storm is associated with a complex solar wind flow produced by multiple interacting ICMEs arising from multiple halo CMEs launched from the Sun in a short period; (3) C-type, in which the storm is associated with a CIR formed at the leading edge of a high-speed stream originating from a solar coronal hole (CH). For the 88 major storms, the S-type, M-type, and C-type events number 53 (60%), 24 (27%), and 11 (13%), respectively. For the 85 events for which the surface source regions could be investigated, 54 (63%) of the storms originated in solar active regions, 11 (13%) in quiet Sun regions associated with quiescent filaments or filament channels, and 11 (13%) were associated with coronal holes. Remarkably, nine (11%) CME-driven events showed no sign of eruptive features on the surface or in the low corona (e.g., no flare, no coronal dimming, and no loop arcade, etc.), even though all the available solar observations in a suitable time period were carefully examined. Thus while it is generally true that a major geomagnetic storm is more likely to be driven by a frontside fast halo CME associated with a major flare, our study indicates a broad distribution of source properties. The implications of the results for space weather forecasting are briefly discussed.

Citation: Zhang, J., et al. (2007), Solar and interplanetary sources of major geomagnetic storms ($Dst \leq -100$ nT) during 1996–2005, *J. Geophys. Res.*, *112*, A10102, doi:10.1029/2007JA012321.

[1]Department of Computational and Data Sciences, George Mason University, Fairfax, Virginia, USA.
[2]NASA Goddard Space Flight Center, Greenbelt, Maryland, USA.
[3]Department of Astronomy, University of Maryland, College Park, Maryland, USA.
[4]Institute for Scientific Research, Boston College, Chestnut Hill, Massachusetts, USA.
[5]Space Science Laboratory, University of California, Berkeley, California, USA.
[6]Kavli Institute for Astrophysics and Space Research, Massachusetts Institute of Technology, Cambridge, Massachusetts, USA.
[7]Lockheed Martin Solar and Astrophysics Laboratory, Palo Alto, California, USA.
[8]Center for Space Plasma and Aeronomic Research, University of Alabama in Huntsville, Huntsville, Alabama, USA.
[9]Catholic University of America, Washington, DC, USA.
[10]Royal Observatory of Belgium, Brussels, Belgium.
[11]Skobeltsyn Institute of Nuclear Physics, Moscow State University, Moscow, Russia.

0148-0227/07/2007JA012321$09.00

1. Introduction

[2] A NASA Living With a Star (LWS) Coordinated Data Analysis Workshop (CDAW) was held at George Mason University, Fairfax, Virginia, in March 2005. A second follow-up CDAW workshop was held at Florida Institute of Technology, Melbourne, Florida, in March 2007. The two workshops focused on the major geomagnetic storms of solar cycle 23, specifically the 88 events from 1996 (corresponding to the start of observations from the SOHO spacecraft) to the end of 2005 having minimum *Dst* (disturbance storm time index) ≤ -100 nT. Four working groups were established to address (1) the solar and interplanetary (IP) sources of these storms, (2) storm mechanisms, (3) the associated ionospheric storms, and (4) storm predictions. Here, we summarize the efforts of Working Group 1 to identify the sequence of Sun-to-Earth activities for all 88 storms. The aim was to produce as comprehensive a list of solar-IP sources as possible by combining a wide variety of data sets and exploiting the different areas of expertize of the group members. The purpose of this paper is to describe the identification methods and present the identification results, which we hope will serve as a basis for further in-depth studies of these important Sun-Earth connection events.

[3] It is now well established that a geomagnetic storm is the consequence of a chain of causative events originating from the Sun and ultimately evolving into a geoeffective solar wind flow in near-Earth space [e.g., *Brueckner et al.*, 1998; *Webb et al.*, 2001; *Berdichevsky et al.*, 2002; *Zhang et al.*, 2003; *dal Lago et al.*, 2004; *Gopalswamy et al.*, 2005]. Such geoeffective solar wind flows fall into two broad types, depending on their origins. One type is associated with IP coronal mass ejections (ICME), the interplanetary counterparts of CMEs at the Sun. An ICME has been conventionally called ejecta and/or magnetic cloud (MC). The latter explicitly refers to a subset of ICMEs in which magnetic fields are enhanced and rotate through a large angle [*Klein and Burlaga*, 1982]. The second type is associated with fast solar wind emanating from solar coronal holes, in particular with the corotating interaction regions (CIRs) that form at the leading edges of such streams as they interact with the preceding slower ambient solar wind. Previous studies have found that major/intense geomagnetic storms (e.g., $Dst \leq -100$ nT, or $Kp \geq 7-$) are mainly caused by ICMEs, while moderate and minor storms can be caused by both ICMEs and CIRs [*Gosling et al.*, 1991; *Tsurutani and Gonzalez*, 1997; *Richardson et al.*, 2002]. Nevertheless, recent studies showed that some major storms may be driven by CIRs [*Zhang et al.*, 2003; *Richardson et al.*, 2006], although their Dst values were not too far below -100 nT. Regardless of the solar origin, the geoeffective solar wind is usually a period of prolonged and enhanced southward directed magnetic field (B_s) that allows efficient solar wind energy transport into the Earth's magnetosphere [e.g., *Dungey*, 1961; *Gonzalez et al.*, 1994]. This enhanced B_s field could be embedded within any part (front or rear) of ICMEs, SHs, and CIRs [e.g., *Crooker et al.*, 1992; *Wu and Lepping*, 2002; *Huttunen and Koskinen*, 2004; *Richardson et al.*, 2006].

[4] Routine associations between ICMEs observed in geospace and CMEs observed at the Sun became possible after the launch of the SOHO spacecraft. Because of unfavorable launching directions and limited angular spans, the majority of CMEs do not intercept the Earth. However, a frontside halo CME, which appears as an expanding circular feature surrounding the coronagraph occulting disk and thus likely has a component moving towards the Earth along the Sun-Earth line, is likely to produce an ICME at the Earth [*Howard et al.*, 1982]. Comprehensive association work, based on a large number of CMEs and ICMEs continuously observed over years, have been carried out [e.g., *Lindsay et al.*, 1999; *Gopalswamy et al.*, 2000; *Cane and Richardson*, 2003; *Schwenn et al.*, 2005]. In general, based on existing solar and solar wind observations, one is able to make unique CME-ICME association for about half of all ICME events. However, reliable one-to-one associations for other ICMEs becomes more difficult, mainly because multiple activity at the Sun results in complex interplanetary flows or compound streams [*Gopalswamy et al.*, 2001; *Burlaga et al.*, 2002; *Zhang et al.*, 2003] or provides several plausible candidate associations. Further, a number of ICMEs, including those causing major geomagnetic storms, were found not to be associated with any identifiable frontside halo CMEs [*Zhang et al.*, 2003; *Schwenn et al.*, 2005].

[5] In this paper, our focus is to identify the solar and IP sources that lead to major geomagnetic storms. Our comprehensive search for the sequence of events includes the solar surface sources, flare activities, CMEs, ICMEs, and CIRs. Various tracking methods are used to address not only the obvious one-to-one events but also to provide the possible sequences for all complex events and events without obvious frontside halo CMEs as well. While the evolution of an event is from the Sun to the Earth, it is practical to work backward from the Earth to the Sun for reliable identifications. The organization of the paper is as follows: Section 2 discusses the selection of major geomagnetic storms. In section 3, we describe the methods used to identify the IP and solar sources of these geomagnetic storms. In section 4, we list the properties of the identified solar and IP sources and discuss the statistical results. Section 5 summarizes the results.

2. Selection of Major Geomagnetic Storms

[6] The workshops focused on the major geomagnetic storms that occurred between January 1996 and December 2005. This 10-year period extends from the start to late in the declining phase of solar cycle 23, which had two sunspot maxima in 2000 and 2001. The *Dst* index is a measure of the strength of the ring current and widely used for measuring the intensity of geomagnetic storms. We defined a major geomagnetic storm as a minimum in the hourly *Dst* index falling below -100 nT. A similar threshold for major/intense storms has been used by other authors [e.g., *Tsurutani et al.*, 1997]. Other indices may be used, such as the *Kp* index [e.g., *Gosling et al.*, 1991; *Richardson et al.*, 2002]. Further, if a period of high activity showed multiple $Dst \leq -100$ nT minima, we arbitrarily assigned these to a single storm event if the minima were separated by less than 24 hours, rather than define each minimum as a separate storm (except for the two storms that occurred at 1200 UT, 6 August, and 0600 UT, 7 August 1998, which corresponded to two well separated ICMEs). As will be

Table 1. Solar and Interplanetary Sources of the 88 Major Geomagnetic Storms During 1996–2005

1	2	3	4	5	6	7	8	9	10	11	12	13	14	15	16
	Dst, min		S-IP[b]	CME								ICME			
ID[a]	Time, UT	Int., nT	Driver Type	Time,[c] UT	Vel, km/s	AW (d)	Flare Class	Source[d] (Region Type)	Source[e] Coord.	IP Solar Wind[f] Structure (Type)	Shock[g] Time, UT	Start, UT	End, UT	CL[h]	FN[i]
1	1996/10/23 0500	−105	C	10/20 0703(CH)	..	..	..	CH	S10	CIR	..	..	..	1	
2	1997/04/22 0000	−107	S	04/16 0735	87	113	NO	UNK	UNK	MC	04/21 0600	04/21 1000	04/23 0400	3	F
3	1997/05/15 1300	−115	S	05/12 0530	464	360	C1.3	AR8038	N21W08	SH+ MC	05/15 0115(W)	05/15 0900	05/16 0000	1	
4	1997/10/11 0400	−130	S	10/06 1528	293	174	NO	QS	S27W05	SH+ MC	10/10 1557(W)	10/10 2200	10/12 0000	1	F
5	1997/11/07 0500	−110	S	11/04 0610	785	360	X2.1	AR8100	S14W33	SH+MC	11/06 2202(A)	11/07 0400	11/08 1000	1	
6	1997/11/23 0700	−108	S	11/19 1700(F)	..	..	C1.6	AR8108	N20E05	SH+ MC	11/22 0912(W)	11/22 1800	11/23 1400	2	F
7	1998/02/18 0100	−100	S	02/12 1555	63	126	No	UNK	UNK	MC	02/17 0400	02/17 1000	02/17 2100	3	F
8	1998/03/10 2100	−116	C	03/08 0903(CH)	..	..	NO	CH	S30	CIR	..	..	..	1	
9	1998/05/04 0600	−205	M	05/02 1406	938	360	X1.1	AR8210	S15W15	PICME-SH	05/04 0215(A)	..	..	2	F
			..	05/02 0531	542	360	C5.4	AR8210	S19W09	..	..	..	..	..	
			..	05/01 2340	585	360	M1.2	AR8210	S18W04	..	..	..	..	..	
			..	04/29 1659	1374	360	M6.8	AR8210	S18E20	..	05/01 2121(W)	05/02 0500	05/04 0200	..	
10	1998/06/26 0500	−101	M	06/22 0734	289	119	NO	QS	S58W05	MC	06/25 1543(A)	06/25 2300	06/26 1900	2	F
			..	06/21 0535	192	163	NO	AR8243	N15W30	..	06/24 1000	06/24 1600	06/25 2300	..	
11	1998/08/06 1200	−138	M	DG	..	..	NO	DG	DG	PICME-SH	08/06 0716(W)	08/05 1300	08/06 1200	3	F
12	1998/08/07 0600	−108	C	DG	..	..	NO	CH	DG	CIR	..	..	..	2	F
13	1998/08/27 1000	−155	S	08/24 2150(F)	..	..	X1.0	AR8307	N35E09	SH+ ICME	08/26 0640(W)	08/26 2200	08/28 0000	1	F
14	1998/09/25 1000	−207	S	09/23 0640(F)	..	..	M7.1	AR8340	N18E09	SH+ MC	09/24 2320(W)	09/25 0200	09/26 1600	1	F
15	1998/10/19 1600	−112	S	10/15 1004	362	360	NO	QS	N10E10	SH+ MC	10/18 1900(A)	10/19 0400	10/20 0700	1	F
16	1998/11/08 0700	−149	M	11/04 0754	523	360	C5.2	AR8375	N17E01	SH+ICME+ PICME-SH	11/07 0736(A)	11/07 2200	11/09 0300	2	F
			..	11/05 2044	1119	360	M8.4	AR8375	N22W18	..	11/08 04:41(W)	..	..	..	
17	1998/11/09 1800	−142	S	11/05 2044	1119	360	M8.4	AR8375	N22W18	MC	11/08 0441(W)	11/09 0400	11/10 0600	1	
18	1998/11/13 2200	−131	S	11/09 1817	325	190	NO	QS	N18E00	MC	11/13 0143 (SC)	11/13 0400	11/14 1200	1	F
19	1999/01/14 0000	−112	S	DG	..	..	NO	DG	DG	SH+ ICME	01/13 1047(W)	01/13 1500	01/13 2300	3	F
20	1999/02/18 1000	−124	S	02/16 0249(F)	..	..	M3.2	AR8458	S23W14	SH+ MC	02/18 0248(W)	02/18 1000	02/19 1100	2	F
21	1999/09/23 0000	−173	S	09/20 0606	604	360	C2.8	QS	S21W05	ICME	09/22 1209(W)	09/22 1900	09/24 0200	1	
22	1999/10/22 0700	−237	S	10/18 0006	144	240	No	QS	S26E08	ICME - CIR	10/21 0220(W)	10/21 0800	10/22 0700	1	
23	1999/11/13 2300	−106	M	DG	..	..	..	DG	DG	ICME+ PICME-SH	11/13 1248(W)	11/12 1000	11/13 1800	3	F
24	2000/02/12 1200	−133	S	02/10 0230	944	360	C7.3	AR8858	N22E03	SH+ ICME	02/11 2334(W)	02/12 0900	02/13 0000	1	
25	2000/04/07 0100	−288	S	04/04 1632	1188	360	C9.7	AR8933	N16W66	SH+ICME	04/06 1632(W)	04/07 0400	04/08 0600	1	
26	2000/05/24 0900	−147	M	05/20 0626	557	..	C7.6	AR8998	S15W08	ICME- ICME	05/22 1700	05/23 0900	05/23 2100	2	F
			..	05/22 0150	649	360	C6.3	AR9004	N20W22	..	05/23 2342(W)	05/24 1200	05/26 1800	..	
27	2000/07/16 0100	−301	S	07/14 1054	1674	360	X5.7	AR9077	N22W07	SH+ MC	07/15 1415(W)	07/15 1900	07/17 0800	1	
28	2000/08/11 0700	−106	S	08/06 2306	281	133	NO	UNK	UNK	SH+ MC	..	08/10 1900	08/12 0100	3	F
29	2000/08/12 1000	−235	S	08/09 1630	702	360	C2.3	AR9114	N11W11	SH+ MC	08/11 1849(W)	08/12 0500	08/13 2200	1	
30	2000/09/18 0000	−201	M	09/16 0518	1215	360	M5.9	AR9165	N14W07	SH(M)+ICME(M)	09/17 1500	09/17 2100	09/21 1200	2	
			..	09/15 2150	285	360	C7.4	AR9165	N12E04	..	..	..	..	..	
			..	09/15 1526	481	217	M2.0	AR9165	N12E07	..	..	..	..	..	
			..	09/15 1206	633	235	C9.5	AR9165	N13E08	..	..	..	..	..	
31	2000/10/05 1400	−182	M	09/29 2150	173	274	NO	UNK	UNK	MC+PMC-SH+ ICME	10/03 0102(W)	10/03 1000	10/05 0600	3	F
			..	10/01 1750	586	136	C5.0	QS	S27E33	..	10/05 0328(W)	10/05 1300	10/07 1100	..	
32	2000/10/14 1500	−107	S	10/09 2350	798	360	C6.7	AR9182	N01W14	SH+ MC	10/12 2233(W)	10/13 1200	10/14 2000	1	
33	2000/10/29 0400	−127	S	10/25 0826	770	360	C4.0	QS	N06W60	SH+ MC	10/28 0930(W)	10/28 2100	10/29 2200	1	F
34	2000/11/06 2200	−159	S	11/03 1826	291	360	NO	UNK	UNK	SH+MC	11/06 0930 (W)	11/06 2200	11/07 1700	3	F
35	2000/11/29 1400	−119	M	11/26 1706	980	360	X4.0	AR9236	N18W38	ICME(M)	11/28 0525 (W)	11/28 1600	11/29 2200	2	F
			..	11/25 1931	671	360	X1.9	AR9236	N20W23	..	..	..	..	..	
36	2001/03/20 1400	−149	S	03/16 0350	271	281	NO	UNK	UNK	SH+ MC	03/19 1133(W)	03/19 1700	03/22 0600	3	F
37	2001/03/31 0900	−387	M	03/29 1026	942	360	X1.7	AR9393	N20W19	SH(M)+ICME(M)	03/31 0114(W)	03/31 0500	04/03 1500	2	

Table 1. (continued)

1	2	3	4	5	6	7	8	9	10	11	12	13	14	15	16
	Dst, min		S-IP[b]	CME								ICME			
ID[a]	Time, UT	Int., nT	Driver Type	Time,[c] UT	Vel, km/s	AW (d)	Flare Class	Source[d] (Region Type)	Source[e] Coord.	IP Solar Wind[f] Structure (Type)	Shock[g] Time, UT	Start, UT	End, UT	CL[h]	FN[i]
			..	03/28 1250	519	360	M4.3	AR9393	N16E03	..	..	..	..	..	
38	2001/04/12 0000	−271	M	04/10 0530	2411	360	X2.3	AR9415	S23W09	SH(M)+MC(M)	..	04/11 2200	04/13 0700	2	
			..	04/09 1554	1192	360	M7.9	AR9415	S21W04	..	..	..	..	..	
39	2001/04/18 0700	−114	S	04/15 1406	1199	167	X14.4	AR9415	S20W85	SH+MC	04/18 0049(W)	04/18 1200	04/20 1100	1	F
40	2001/04/22 1600	−102	S	UNK	..	..	NO	UNK	UNK	MC	04/21 1529(W)	04/21 2300	04/23 0800	3	F
41	2001/08/17 2200	−105	S	08/14 1601	618	360	C2.3	AR9577	N16W36	SH+MC	08/17 1101(W)	08/17 2000	08/19 1600	1	
42	2001/09/26 0200	−102	S	09/24 1030	2402	360	X2.6	AR9632	S16E23	SH+ICME	09/25 2017(W)	..	..	1	
43	2001/10/01 0900	−148	S	09/28 0854	846	360	M3.3	AR9636	N08E19	SH+ICME	09/30 1914(W)	10/01 0800	10/02 0000	1	
44	2001/10/03 1500	−166	S	09/29 1154	509	216	M1.8	AR9636	N13E03	MC	10/01 2200	10/02 0400	10/03 1700	1	
45	2001/10/21 2200	−187	S	10/19 1650	901	360	X1.6	AR9661	N15W29	SH+ICME	10/21 1640(W)	10/21 2000	10/25 1000	1	
46	2001/10/28 1200	−157	M	10/25 1526	1092	360	X1.3	AR9672	S18W19	PICME-SH	10/28 0313(W)	..	..	2	
			..	10/24 0626	597	145	C2.6	AR9675	S13E27	..	10/26 2200	10/27 0300	10/28 2000?	..	
47	2001/11/06 0700	−292	M	11/04 1635	1810	360	X1.0	AR9684	N06W18	MC+ PMC-SH+ICME	11/06 0125(A)	11/06 1300	11/09 0600	2	F
			..	11/03 1920	457	360	NO	DG	DG	..	11/05 1000	11/05 1900	11/06 0600	..	
48	2001/11/24 1700	−221	M	11/22 2330	1437	360	M9.9	AR9704	S14W36	SH(M)+ICME	11/24 0454(W)	11/24 1400	11/26 0000	2	
			..	11/22 2030	1443	360	M3.8	AR9698	S25W67	..	11/24 0551(W)	..	..	..	
49	2002/03/24 1000	−100	M	03/19 1154	860	180	M1.0	AR9866	S10W58	SH(M)+ICME(M)	03/23 1124(W)	03/23 2100	03/25 2000	2	
			..	03/20 1754	603	180	NO	AR9871	S21W15	..	..	..	..	..	
50	2002/04/18 0800	−127	S	04/15 0350	720	360	M1.2	AR9906	S15W01	SH+ MC	04/17 1101(W)	04/17 1600	04/19 1500	1	
51	2002/04/20 0900	−149	S	04/17 0826	1240	360	M2.6	AR9906	S14W34	SH+ MC	04/19 0825(W)	04/20 0000	04/21 1800	1	F
52	2002/05/11 2000	−110	S	05/08 1350	614	360	C4.2	AR9934	S12W07	SH+ICME	05/11 1130	05/11 1600	05/12 0000	1	
53	2002/05/23 1800	−109	M	05/22 0006	1246	186	C9.7	AR9948	S25W64	SH(M)	05/23 1044(W)	05/23 2000	05/25 1800	2	
			..	05/22 0350	1557	360	C5.0	QS	S22W53	..	..	..	..	..	
54	2002/08/02 0600	−102	M	07/29 1207	562	154	NO	QS	N34W36	ICME+ PICME-SH+MC	08/01 0424(A)	08/01 0900	08/02 0000	3	F
55	2002/08/21 0700	−106	S	08/16 1230	1585	360	M5.2	AR0069	S14E20	SH+ MC	08/20 1300	08/20 1500	08/21 1400	2	F
56	2002/09/04 0600	−109	C	08/31 0648(CH)	..	..	..	CH	S15	CIR	..	..	..	1	F
57	2002/09/08 0100	−181	M	09/05 1654	1748	360	C5.2	AR0102	N09E28	PICME-SH+ICME	09/07 1622(W)	09/08 0400	09/08 2000	3	F
	..	..	..	..	..	..	..	..	..	..	..	09/07 10	09/08 04	..	
58	2002/10/01 1700	−176	S	09/26 0131	178	202	NO	UNK	UNK	SH+ MC+CIR	09/30 0754(W)	09/30 2000	10/02 0300	3	F
59	2002/10/04 0900	−146	S	09/30 0230	258	120	NO	QS	S17W17	SH+ MC	10/02 2241(W)	10/03 0100	10/04 1800	1	F
60	2002/10/07 0800	−115	C	10/05 0148(CH)	..	..	..	CH	S07	CIR	..	..	..	1	
61	2002/10/14 1400	−100	C	10/11 0239(CH)	..	..	..	CH	S26	CIR	..	..	..	1	
62	2002/11/21 1100	−128	C	11/18 1321(CH)	..	..	..	CH	S04	CIR	11/20 1049(W)	..	..	1	F
63	2003/05/30 0000	−144	M	05/28 0050	1366	360	X3.6	AR0365	S11W12	SH(M)+ICME(M)	05/29 1155(A)	05/29 1300	05/29 1800	2	F
			..	05/27 2350	964	360	X1.3	AR0365	S0W17	..	05/29 18:31(W)	05/30 02	05/30 16	..	
			..	05/27 0650	509	360	M1.6	AR0365	S07W14	..	..	..	..	..	
64	2003/06/18 1000	−141	M	06/14 0154	875	195	NO	QS	N22W15	SH(M)+ICME(M)+ PICME-SH	06/16 1800	06/17 0700	06/18 0900	2	F
			..	06/15 2354	2053	360	X1.3	AR0386	S07E80	..	06/18 04:42(W)	..	..	..	
65	2003/07/12 0600	−105	C	07/07 2140(CH)	..	..	..	CH	N04	CIR	..	..	..	1	
66	2003/08/18 1600	−148	S	08/14 2006	378	360	NO	QS	S30E00	SH+ MC	08/17 1345(A)	08/18 0100	08/19 1500	2	F
67	2003/10/30 0100	−353	S	10/28 1130	2459	360	X17.2	AR0486	S16E08	SH+ MC	10/29 0558(W)	10/29 1100	10/30 0300	1	F
68	2003/10/30 2300	−383	S	10/29 2054	2029	360	X10.0	AR0486	S15W02	SH+MC	10/30 1619(W)	10/31 0200	11/02 0000?	1	
69	2003/11/20 2100	−422	S	11/18 0850	1660	360	M3.9	AR0501	N00E18	SH+ MC	11/20 0835(W)	11/20 1000	11/21 0100	1	F
70	2004/01/22 1400	−149	S	01/20 0006	965	360	C5.5	AR0540	S13W11	SH+ ICME	01/22 0105(A)	01/22 0800	01/23 1700	1	F
71	2004/02/11 1800	−109	C	02/10 0924(CH)	..	..	..	CH	N02	CIR	..	..	..	1	
72	2004/04/04 0100	−112	S	03/31 1036(F)	..	..	C3.4	AR0582	N16W10	SH+MC	04/03 0900(A)	04/04 0000	04/05 1800	2	F
73	2004/07/23 0300	−101	S	07/20 1331	710	360	M8.6	AR0652	N10E35	SH+ ICME	07/22 0945(W)	07/22 1800	07/24 0800	1	F

Table 1. (continued)

1	2	3	4	5	6	7	8	9	10	11	12	13	14	15	16
	Dst, min		S-IP[b]	CME								ICME			
ID[a]	Time, UT	Int., nT	Driver Type	Time,[c] UT	Vel, km/s	AW (d)	Flare Class	Source[d] (Region Type)	Source[e] Coord.	IP Solar Wind[f] Structure (Type)	Shock[g] Time, UT	Start, UT	End, UT	CL[h]	FN[i]
74	2004/07/25 1200	−148	S	07/22 0830	899	132	C5.3	AR0652	N02E08	SH+ MC	07/24 0532(W)	07/24 1400	07/25 1500	1	F
75	2004/07/27 1400	−197	S	07/25 1454	1333	360	M1.1	AR0652	N04W30	SH+ MC	07/26 2225(W)	07/27 0200	07/27 1500	1	
76	2004/08/30 2300	−126	S	08/25 1331	108	182	NO	UNK	UNK	MC+CIR	08/29 0909(W)	08/29 1900	08/30 2200	3	F
77	2004/11/08 0700	−373	M	11/04 2330	1055	293	M5.4	AR0696	N08E18	SH(M)+ MC(M)	11/07 0155(A)	11/07 2200	11/09 1000	2	
			..	11/04 0954	653	360	C6.3	AR0696	S09E28	..	11/07 17:59(W)	..	..	..	
78	2004/11/10 1000	−289	M	11/07 1654	1759	360	X2.0	AR0696	N09W17	PICME-SH+ MC	11/09 0925(W)	11/09 2000	11/23 2000	2	F
			..	11/06 0206	1111	214	M9.3	AR0696	N09E05	..	..	..	..	..	
79	2005/01/18 0800	−121	M	01/15 2306	2861	360	X2.6	AR0720	N16W05	SH(M)	01/17 0715(A)	..	..	2	F
			..	01/15 0630	2049	360	M8.6	AR0720	N16E04	..	..	..	..	..	
80	2005/01/22 0600	−105	S	01/20 0654	882	360	X7.1	AR0720	N12W58	SH + ICME	01/21 1652(A)	01/21 2000	01/22 1700	1	
81	2005/05/08 1400	−127	C	05/07 0136(C)	..	..	..	CH	N10	CIR	..	..	..	1	
82	2005/05/15 0800	−263	S	05/13 1712	1128	360	M8.0	AR0759	N12E12	SH+ MC	05/15 0211(A)	05/15 0600	05/17 1200	1	
83	2005/05/20 0900	−103	S	05/16 1350	405	360	C1.2	AR0759	N13W29	ICME	..	05/20 0400	05/21 0500	1	F
84	2005/05/30 1000	−138	S	05/26 1506	586	360	B7.5	AR0767	S12E13	ICME	05/29 0905(A)	05/31 0100	05/30 2300	2	F
85	2005/06/12 2300	−105	S	06/09 1436	377	125	C1.4	AR0772	S15W58	MC	06/12 0400(A)	06/12 1600	06/13 1300	2	F
86	2005/08/24 1100	−216	M	08/22 0131	1194	360	M2.6	AR0798	S11W54	SH(M) + ICME(M)	08/24 0545(A)	..	..	2	
			..	08/22 1730	2378	360	M5.6	AR0798	S12W60	..	..	..	..	..	
87	2005/08/31 1600	−131	C	08/29 1048(C)	..	..	..	CH	S12	CIR	..	..	..	1	
88	2005/09/11 1100	−147	S	09/09 1948	2257	360	X6.2	AR0808	S10E58	SH+ ICME	09/11 0100(A)	09/11 0500	09/12 0700	1	F

[a]Event number in chronological order.

[b]Solar and IP sources type: S - single CME/ICME, M - multiple CMEs/ICMEs, C - Coronal Hole/CIR.

[c]Time of first CME appearance in LASCO C2, except for (F), the onset time of the source flare, and (CH), the central meridian crossing time of the source coronal hole. "UNK" source unknown, "DG" LASCO data gap.

[d]Solar surface source region indicated by the NOAA active region number, or CH for a coronal hole, QS for a quiet Sun region, UNK if the source region can not be identified in the available observations, and DG for the EIT data gap.

[e]Surface source region heliographic coordinates. In the case of coronal holes, only the latitude is given. UNK and DG are defined as in footnote d.

[f]Solar wind structures associated with the geomagnetic storm in time order. SH = sheath; ICME = interplanetary CME; MC = magnetic cloud. (M) indicates multiple structures of this type. "-" indicates an interaction between two structures, in particular, PICME-SH and PMC-SH denote a shock propagating through a preceding ICME or magnetic could respectively. Bold type indicates the structure associated with the peak of the storm; other structures that contribute to the storm (typically at the $\geq\sim -100$ nT level) are indicated in the normal type.

[g]Shock passage time at ACE (A), WIND (W) or inferred from a geomagnetic storm sudden commencement (SC). If no shock is present, this is the arrival time of CME-driven disturbances.

[h]Overall confidence level on the identification of solar sources."1" unambiguous with unanimous consensus from our group members. "2" less unambiguous with optional choice of sources, but most of group members agree on the identification listed. M-type events automatically fall into this category because of the intrinsic complexity. "3" ambiguous events and problematic events. Events in this category are mostly driven by ICMEs but no obvious front-side halo CME counterpart identified. The CMEs listed are the possible candidates but ones without any surface signature in the available observations, as indicated by "UNK" in column 9 and 10. See the footnotes and text for more discussion on the questionable events.

noted later, both single and multiple solar CMEs were found to be responsible for minima within a "single" storm event.

[7] We identified 88 major geomagnetic storms in total from January 1996 to December 2005, using the selection criteria described above. The events through 2003 are based on the final *Dst* index, whereas those in 2004 and 2005 are based on the provisional *Dst* index, so it is possible that they may be adjusted slightly based on the final index. (*Dst* data are obtained at http://swdcdb.kugi.kyoto-u.ac.jp/dstdir/index.html). The 88 storms are listed in Table 1, where the first three columns indicate the event reference number, the storm peak time, and the minimum *Dst* value, respectively. The other columns, which will be explained later, describe the parameters for the solar and IP sources.

[8] Figure 1 shows the distributions of the storm strength (Figure 1a), yearly occurrence rate (Figure 1b), and occurrence rate as a function of calendar month (Figure 1c). A majority of these events (60 out of 88; 68%) had minimum *Dst* between −100 nT and −150 nT. A further 10 events (11%) had minimum *Dst* between −150 nT and −200 nT. There were 18 "severe" storms (21%) with minimum $Dst \leq -200$ nT. The largest geomagnetic storm ($Dst = -422$ nT) occurred on 20 November 2003 [*Gopalswamy et al.*, 2005]. The yearly major storm occurrence rate was highest (∼13 events per year) during 2000–2002 around the time of maximum sunspot number (SSN). The occurrence rate was lowest in 1996 at solar minimum. Figure 1c shows that the occurrence of major storms in general followed the well-known semiannual variation of geomagnetic activity [e.g., *Russell and McPherron*, 1973; *Cliver et al.*, 2002], that is, higher activity during the equinoctial months and lower activity around the solstitial months. The number of major storms peaked in April–May and in October–November and was lowest in June and in December (when no storms occurred). The number of major storms around the fall equinox was almost twice that at the spring equinox with 55 events during the second half of the year compared with only 33 during the first half. A similar seasonal asymmetry of the occurrence of "very intense" storms has been reported before [*Gonzalez et al.*, 2002].

3. Methods of Identifying Solar-IP Sources of Major Storms

3.1. Identifying and Characterizing the IP Sources

[9] The primary physical mechanism for energy transfer from the solar wind to the magnetosphere is magnetic reconnection between the IMF and the Earth's magnetic field. The efficiency of this process mainly depends on the strength of the southward IMF, or more accurately, the dawn-dusk (y) component of the electric field ($\mathbf{E} = -\mathbf{V} \times \mathbf{B}$) [e.g., *Dungey*, 1961; *Perreault and Akasofu*, 1978; *Tsurutani and Gonzalez*, 1997]. One formulation for the *Dst* index [*O'Brien and McPherron*, 2000] relates the (pressure-corrected) *Dst** index to the solar wind driver given by VB_s, where VB_s is the rectified value of VB_z that is

Notes to Table 1.

[i]Additional comments are in the footnote numbered according to the event number as follows: (2) Proposed CME 04/16 07 had no corresponding surface eruption signature in EIT. An alternative solar driver is an EIT dimming at 04/16 1400 UT at S22E04. However, this dimming has no corresponding CME in LASCO. (4) Filament eruption, no EIT dimming. The surface source region is near NOAA AR8090. (6) LASCO/EIT data gap, but C1 LDE flare, and cusp in SXT. (7) Proposed CME 02/12 15 had no corresponding surface eruption signature in EIT. Partial halo CME 02/14 0600 is too close to the ICME arrival time because the slow solar wind and slow CME speed imply a longer transit time. (9) A complex flow event involving multiple CMEs/ICMEs. The onset of this flow was caused by CME 04/29 1700. The shock associated with the principle CME (05/02 14) driving the storm arrived at 05/04 0215(A). (10) Storm driven by the second MC. EIT data gap. Surface sources inferred from SXI. (11) LASCO/EIT data gap. No major flare activity. (12) LASCO/EIT data gap. No major flare activity. (13) LASCO/EIT data gap. X1.0 LDE flare. (14) LASCO/EIT data gap. M7.1 LDE flare. (15) Slow filament eruption. (16) Bs mainly in the first ICME. (18) The source region is in the quiet Sun between two active regions. (19) LASCO/EIT data gap. No major flare activity. (20) LASCO/EIT data gap. M3.2 flare. (23) LASCO/EIT data gap. (26) Both CMEs are not in the original catalog. LASCO images indicated multiple CMEs interacting in the field of view. (28) Surface source region of the 08/06 2300 UT has not been identified. Maybe it is a backside CME? An alternative driver is the CME at 08/08 1500 UT, but the source region is at N25W75, and this may be difficult to reconcile with a MC counterpart at the Earth. (31) Three < −100 nT minima, caused by the magnetic cloud, a shock running into this magnetic cloud, and an ICME. (33) Surface source region showed weak dimming in EIT. It was between two active regions. (34) Surface source region largely unknown. One possibility is a large-scale dimming spanning four small active regions, AR 9218, 9213, 9212, and 9214 with a centroid at N10E05. (35) Three FH CMEs on 11/24 may be also involved in the early part of the complex solar wind flow. (36) CME 03/16 0300 UT lacked a disc signature in EIT. So it maybe a backside CME. An alternative source is the EIT eruption at 03/15 2100 UT. However, it did not produce a CME in LASCO. (39) Big SEP, LASCO snowstorm. However, is the near-limb source consistent with the MC present at 1 AU? An alternative source would be PH CME at 04/14 2100 UT from N45E15. (40) No good solar driver can be found. Filament eruption at 04/17 1300 UT close to southern polar region, however, it produced a narrow and weak CME unlisted in the CME Catalog. PH CME at 04/19 1200 UT from N19W22 corresponded to a transit time of about 50 hours, which was inconsistent with the slow ICME and CME speed. (47) EIT data gap. (51) Double Dst peak. (54) GOES M4.7 flare at 07/29 1027 UT was not associated with CME 07/29 1200 UT. Another CME source for this M-type event is not clear. (55) PH CME 08/18 2100 UT was too slow, not compatible with a 1000 km/s transit speed. However, CME 08/16 1200 must have slowed down significantly before reaching the Earth, possibly affected by a preceding CME. (56) EIT data gap. CH central meridian transit time was extrapolated from earlier observations. (57) M-type, what is the other solar CME? FH CME at 09/05 1600 UT showed EIT dimming, wave and arcade. (58) The CME was a gradual one, growing more prominent in C3 than in C2. However, there was no apparent eruption signature seen in EIT. CIR was involved in the SW flow. CME at 09/28 1100 UT could be an alternative? It seemed too close to the ICME arrival. (59) CME not in the original CDAW catalog. (62) EIT data gap. CH central meridian transit time was extrapolated from earlier observations. (63) SMEI halo CME (best one); 5/28, 1653 thru 5/29. EIT 304 instead of EIT 195 observations. (64) SMEI CME. EIT arcade associated with PH CME 06/14 0100 UT. (66) Strong halo CME, but no dimming, no flare. EIT showed weak wave originated at S30E00, which might be the surface source region of the CME. However, this is not conclusive because of the lack of definite signatures. (67) Two Dst dips. (69) SMEI CME 11/19, 0548. 50–75°. (70) SMEI CMEs on 1/21, 0349 and 22, 0414. 35–80°. (72) C3.4 LDE flare. Eruption seen in SXI. LASCO/EIT data gap. Halo CME in C3 at 04/01 0025 UT. Sheath and cloud boundary unclear. SMEI CMEs 3/31 to 4/3. Out to 90°. (73) Complete chain is shown with SMEI. Shock and cloud boundary unclear. (74) SMEI CME loops at 7/20, 2129 and 21, 1602 match LASCO CME structure well. (76) CME 08/25 13 UT gradual type. It had apparent eruption signature seen in EIT. Could be a frontside CME? Or backside? An alternative driver is CME at 08/26 1200 UT. However, the transit time was probably too short, not compatible with the CME speed and ICME speed. (78) SMEI CME 11/8, 1922: several parts or events; 40–85°. (79) No clear ejecta signatures. (83) No CME-driven shock. (84) EIT 304 only. (85) EIT data gap. Surface source region inconclusive. Flare C1.4 had a gradual component. (88) LASCO/EIT data gap from 09/07 to 09/09.

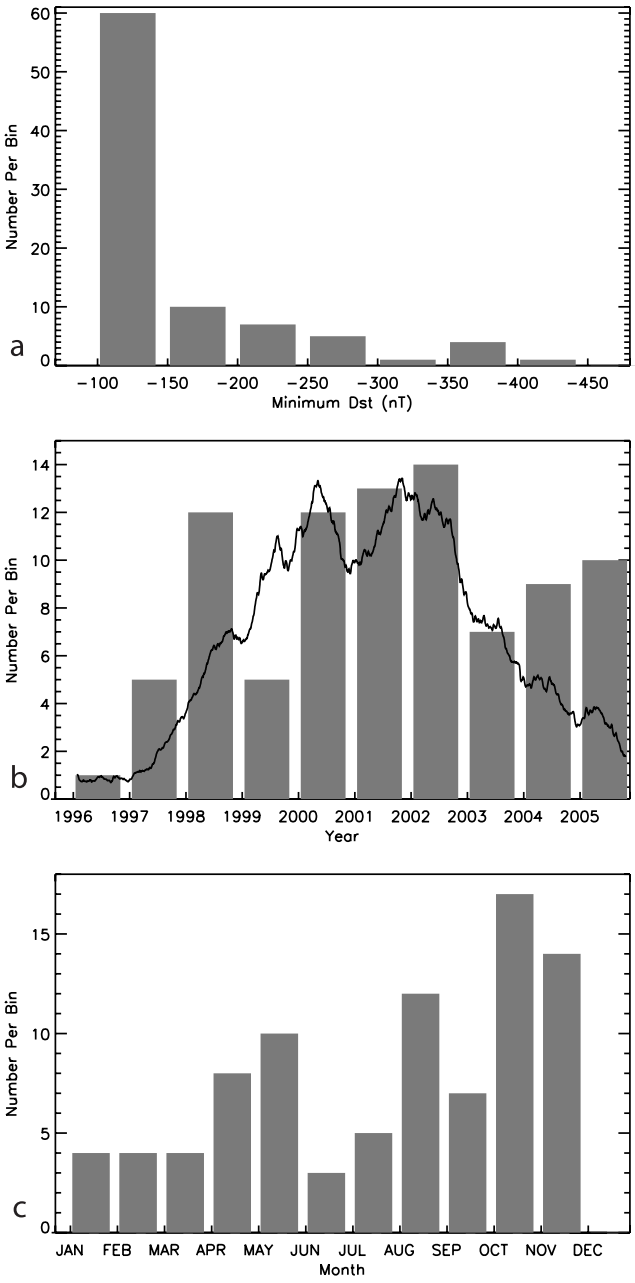

Figure 1. (a) Distributions of the minimum *Dst* (bin size = 50 nT), (b) yearly occurrence rate, and (c) occurrence rate per calender month for 88 major geomagnetic storms during 1996–2005. The black curve overlaid in Figure 1b shows the 180-day-running-average daily sunspot numbers in arbitrary units.

positive when B_z is southward and zero when B_z is northward. The equations are

$$\frac{d}{dt}Dst^* = Q(VB_s) - \frac{Dst^*}{\tau(VB_s)}, \tag{1}$$

$$Q(VB_s) = \begin{cases} \alpha(VB_s - E_c) & VB_s > E_c, \\ 0 & VB_s \le E_c, \end{cases} \tag{2}$$

$$\tau(VB_s) = \tau_\infty \exp\left(\frac{V_o}{V_q + VB_s}\right). \tag{3}$$

The rate of change of *Dst** is assumed to be proportional to VB_s (Q representing injection into the ring current) less a loss term represented by the recovery time τ that depends on the strength of the ring current and is assumed to be proportional to *Dst**.

[10] Since storms are driven by the solar wind magnetic fields and plasma impinging on the Earth, we used in situ solar wind plasma and magnetic field observations from the Advanced Composition Explorer (ACE) and WIND spacecraft to identify the IP sources of the geomagnetic storms in this study. For ACE data, covering events during early 1998–2005, 64-s resolution data were examined. We also examined solar wind ion composition data from the ACE/SWICS instrument. ACE is in orbit at the upstream L1 point, so there is typically a ~20–60 min delay for solar wind structures to transit from ACE to the Earth. For WIND data, 92-s resolution data were used. During the period of this study, WIND spacecraft executed a complicated trajectory in the near-Earth solar wind with a variable solar wind transit time delay of typically less than 1 hour. Because of the near-complete observations provided by the two spacecraft together, we were able to deduce the IP sources for all 88 major geomagnetic storms studied.

[11] On the basis of their plasma and magnetic signatures, we identified various types of structures in the near-Earth solar wind in association with the geomagnetic storms. These include ICME, the upstream ICME-driven shock front, the SH between the shock front and ICME, and CIR. Note that for the sake of clarity on discussions of solar wind structures, ICME here refers to the coherent magnetic structure originating from solar CMEs and thus does not include the SH part. To assist in these identifications, we referred to several existing catalogs. For shocks, we used the WIND shock list compiled by J. Kasper (http://space.mit.edu/home/jck/shockdb/shockdb.html) and the ACE shock list compiled by C. W. Smith (http://www-ssg.sr.unh.edu/mag/ace/ACElists/obs_list.html). For ICMEs, we referred to an updated version of the "comprehensive" ICME list compiled by *Cane and Richardson* [2003]. In addition, we used lists of MCs and "cloud-like" ICMEs compiled by R. P. Lepping and C.-C. Wu (http://lepmfi.gsfc.nasa.gov/mfi/MCL1.html) [*Lepping et al.*, 2005] and the magnetic cloud list of *Huttunen et al.* [2005]. Considering plasma composition and charge states, we used the list of high Fe-charge state intervals that are frequently associated with ICMEs, compiled by *Lepri et al.* [2001], supplemented by information on compositional and charge state anomalies, also typically associated with ICMEs, based on the study of *Richardson and Cane* [2004].

[12] The storm of 27 July 2004 (Event 75 in Table 1) serves to illustrate the method of source identification, as shown in Figure 2. Figure 2a shows the *Dst* index, indicating that this storm had a minimum value of *Dst* = −197 nT at 1400 UT. Figures 2b–2f show time profiles of the IMF strength and north-south (z) component, velocity, proton density, proton temperature, and calculated plasma β, respectively. The three solar images in Figure 2g will be

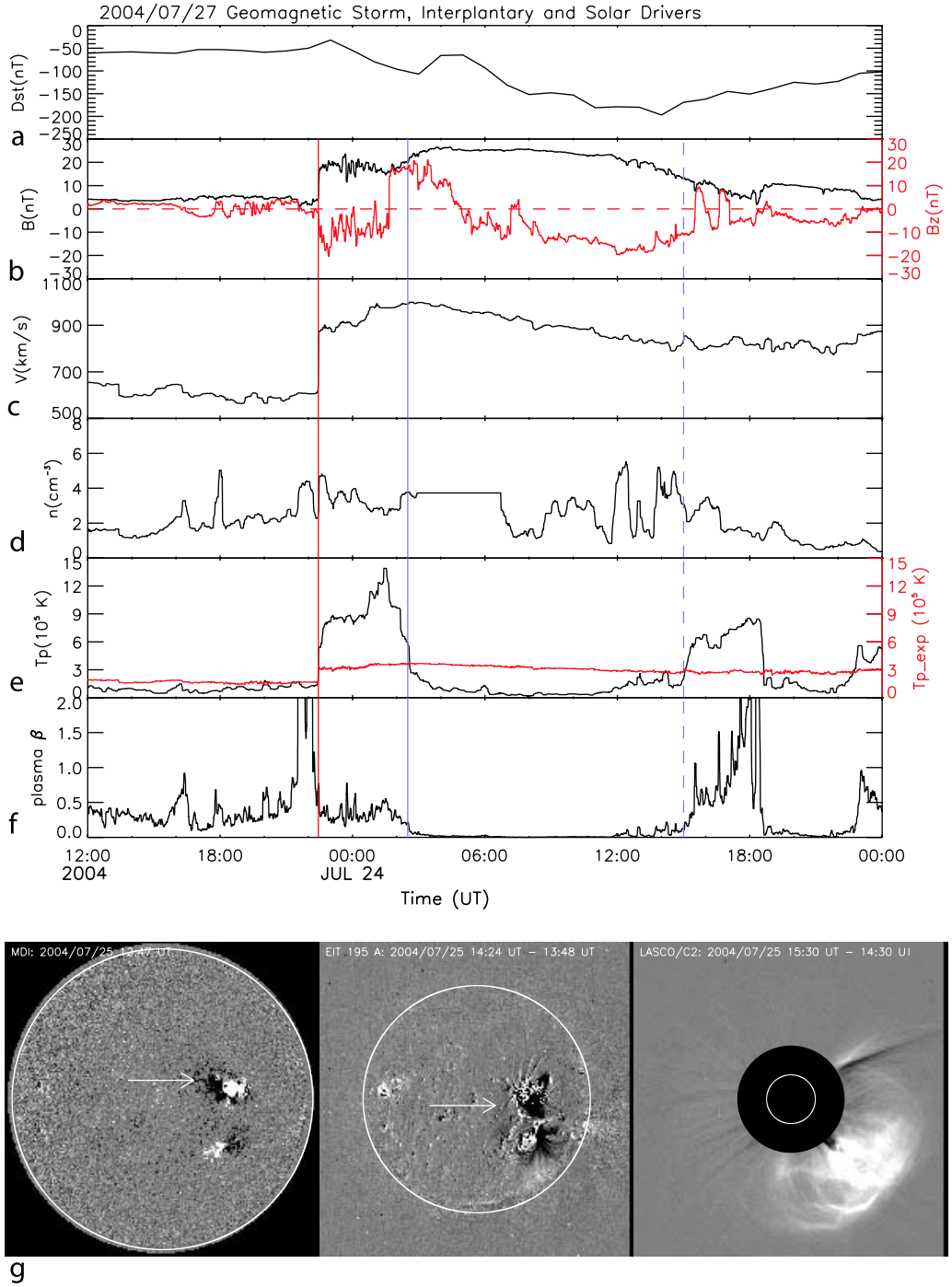

Figure 2. Geomagnetic, interplanetary, and solar data related to the major geomagnetic storm (minimum *Dst* = −197 nT) on 27 July 2004 (event 75), showing (a) temporal profiles of the *Dst* index, (b) solar wind magnetic field intensity (black) with the B_z component (red) overlaid, (c) solar wind velocity, (d) density, and (e) proton temperature (black) overlaid with the expected temperature (red) [*Richardson and Cane*, 1995], and (f) the plasma β. The solar wind data are from ACE in GSE coordinates. The solid and dotted blue vertical lines indicate the starting and ending times of the ICME, which in this case is a magnetic cloud. The vertical red line indicates the arrival time of the ICME-driven shock. (g) The three images, from left to right, indicate the source active region in a SOHO/MDI magnetogram, the coronal dimming accompanying the associated CME observed by EIT (running difference image), and this CME shown in a LASCO C2 coronagraph running difference image.

explained later. The IP driver of the main phase of the storm was evidently the extended interval of southward magnetic field reaching values of ~20 nT that started at ~0500 UT on 27 July and lasted for about 10 hours. There was also a separate interval of southward field from ~2200 UT on 26 July to ~0200 UT on 27 July that depressed *Dst* just below −100 nT at ~3 UT. *Dst* then recovered in response to a northward turning of the IMF; note the ~2 hour delay in the *Dst* response due to the solar wind transit time from ACE and magnetospheric effects.

[13] Examining the broader context of the solar wind driver, we identified the passage of a fast forward IP shock at 2227 UT (at ACE; 2225 UT at WIND) on 26 July (indicated by the vertical red line in Figure 2), characterized by abrupt jumps in the solar wind magnetic field, speed, density, and temperature. The shock was followed by a "sheath" of shocked IP plasma characterized by enhanced, fluctuating field strength, speed, density, and temperature, extending for about 4 hours.

[14] The interval between the two blue vertical lines is the probable time of passage of the ICME that was driving this shock. The signatures of ICMEs have been discussed extensively [e.g., *Neugebauer and Goldstein*, 1997; *Wimmer-Schweingruber et al.*, 2006; *Zurbuchen and Richardson*, 2006]. Here, we note the abnormally low proton temperature, depressed below the expected temperature for normal solar wind [*Richardson and Cane*, 1995] overlaid in red, together with the enhanced magnetic field, smooth rotation in field direction (evident in B_z), and low plasma β that is characteristic of a MC. Other signatures (not shown here) include enhanced oxygen charge states observed by ACE/SWICS and bidirectional suprathermal electron flows observed by the ACE solar wind plasma instrument. Thus the extended region of southward field driving the main phase of this storm was associated with the passage of a MC. The short period of southward field producing the initial phase of the storm was associated with the sheath of shocked plasma ahead of the MC. Compressed magnetic fields in sheath regions may be draped over around the approaching ICME [e.g., *Gosling and McComas*, 1987]. This may lead to strong out-of-the-ecliptic fields, perhaps accounting for the initial phase of this storm. Two notable features of this event are the high solar wind speeds, reaching ~1000 km/s, in the SH and MC, and the overall low solar wind densities compared to average values.

[15] Considering CIRs, regions of compressed plasma formed by the interaction of high-speed streams from coronal holes with the preceding slower solar wind, these can be recognized by their characteristic variations in plasma parameters, including enhancements in the magnetic field strength, plasma density, temperature, and flow deflections lying at the leading edges of corotating high-speed streams [e.g., *Forsyth and Marsch*, 1999, and references therein]. Examples of major storms in our study driven by CIRs have been illustrated by *Richardson et al.* [2006], so a sample event will not be discussed in the present paper. For a recent review of CIRs and associated geomagnetic activity, see the special section in JGR [*Tsurutani et al.*, 2006a] and the AGU Monograph 167 [*Tsurutani et al.*, 2006b].

3.2. Identifying Solar Sources

[16] To identify the solar sources of the IP structures such as ICMEs that drive the major storms studied, we predominantly used observations from instruments on the SOHO spacecraft. CMEs near the Sun are observed by the LASCO C2 and C3 coronagraphs [*Brueckner et al.*, 1995], which have fields of view of $2-6\ R_s$ and $4-30\ R_s$ (measured from the solar disk center in units of solar radius), respectively. There were LASCO observations for 80 of the 88 major geomagnetic storms studied. The eight events with LASCO data gaps occurred mostly in 1998 and 1999 when SOHO lost control for many months. To identify the surface features of CMEs in the source region, observations from SOHO's Extreme-Ultraviolet Imaging Telescope (EIT) [*Delaboudiniere et al.*, 1995], which images the Sun's corona over the full disk and up to 1.5 R_s, were used, in particular those in the 195 Å passband which is dominated by Fe XII emission and sensitive to a plasma temperature of about 1.5 MK. In addition to referring to the LASCO CME catalog generated by NASA and The Catholic University of America in cooperation with the Naval Research Laboratory [*Yashiro et al.*, 2004] (http://cdaw.gsfc.nasa.gov/CME_list/), we also carefully examined all the LASCO and EIT images in a suitable period prior to each storm to search for any eruption features that might not have been included in the catalog and to confirm the nature of the cataloged events. The Michelson Doppler Imager (MDI) [*Scherrer et al.*, 1995] provided photospheric magnetograms.

[17] In addition to SOHO observations, we used "traditional" synoptic data, such as daily NOAA solar event reports, which include data on soft X-ray flares, filament eruptions, and active regions (http://www.sec.noaa.gov/ftpdir/indices/). These data complement and reinforce the SOHO LASCO/EIT observations. We have also used X-ray coronal images made by the Yohkoh Soft X-ray Telescope (SXT) [*Tsuneta et al.*, 1991] while it was available (Yohkoh was permanently lost in December 2001) to search for possible eruption signatures. X-ray imaging observations made by the Soft X-ray Imager (SXI) on the GOES satellites [*Hill et al.*, 2005] have also been used when available. For events from February 2003 onward, observations from the Solar Mass Ejection Imager (SMEI) [*Jackson et al.*, 2004; *Webb et al.*, 2006] were used to help track CMEs to larger distances from the Sun than is possible with LASCO and to aid in the identification and timing of the Earth arrival of the ICME and shock and the storm onset.

[18] The method of identifying the solar source of an ICME is straightforward, though the results are ambiguous in some cases. This method is to find a frontside halo (full or partial) CME at a reasonable earlier time, which depends on the transit time of the CME from the Sun to the Earth [e.g. *Webb et al.*, 2000; *Zhang et al.*, 2003]. The justification of this method is that there must be a cause-and-effect relationship between solar and IP events, even though current observations only cover the near-Sun space, through remote sensing, and the near-Earth space through in situ sampling. Model calculations also show a good correlation between CME structures at the Sun and ICME structures at the Earth [e.g., *Krall et al.*, 2006; *Yurchyshyn et al.*, 2006]. However, for the purpose of identification, the lack of imaging observations in the vast region between the Sun and the Earth through which CMEs can travel for days without direct tracking, contributes to the ambiguity of the association between CMEs and ICMEs.

[19] Among the many CMEs observed at the Sun, halo CMEs, seen as an expanding circular bright feature fully surrounding the coronagraph occulting disk (angular width 360°), are believed most likely to hit the Earth [e.g., *Howard et al.*, 1982]. The large angular width observed is attributed both to the projection effect and a large intrinsic width, indicating that the CME axis is likely to be directed along the Sun-Earth line, either toward the Earth if originating from the frontside of the Sun or away from the Earth if originating from the backside of the Sun. In addition to "full" halo CMEs, we also consider "partial halo" CMEs (apparent angular width $\geq$120°) in the solar source identification. To verify the surface source region of a CME, we mainly use EIT observations, which often manifest the CME origin with several eruptive features, including a large scale coronal dimming [e.g., *Thompson et al.*, 1998] and a posteruption loop arcade (the counterpart of the more familiar postflare loop arcade in H_α). These eruptive features are often associated with localized coronal brightenings (the counterparts of flares at EUV wavelengths).

[20] Considering the complexity in associating CMEs with ICMEs, we exploited an iterative process with multiple steps. First, we found all candidate frontside halo CMEs within a 120-hour-long search window before the arrival time of the ICME-driven shock (or other upstream disturbance if there was no fully developed shock, or the ICME arrival if there was no upstream disturbance). The 120-hour-long search window corresponds to a 1 AU transit speed of 347 km/s and is large enough to cover most possible CME sources except for extremely slow events. The large search window may produce several CME candidates, but further steps help to distinguish between likely and unlikely associations. The next step is to reduce the search window by estimating the CME transit time based on in situ solar wind velocities at the location of shock arrival. Since fast CMEs tend to decelerate when moving through the slower solar wind, this method will give an upper estimate for the travel time. This method is not applicable to slow ICMEs because the corresponding, initially slow, CME may be accelerated by the ambient solar wind. In such cases, the full 120-hour window is used. In some unusual cases where there is no front-side halo CME in the 120-hour window, we extend this window even longer to take into account the extremely slow halo CME (e.g.,<200 km/s) at the Sun (the association of these events is usually problematic as discussed later). The third step is that, for each remaining candidate CME in the search window, we consider whether the CME speed at the Sun is consistent with the 1 AU transit speed implied by an association with the 1 AU shock/ICME and with the in situ solar wind speed.

[21] We recognize that the observed CME speed projected on the plane of the sky may not directly indicate the earthward directed speed. Nevertheless, these speeds tend to be loosely correlated. Comparison with statistical studies of the relationship between CME speeds and 1 AU transit times [e.g., *Cane et al.*, 2000; *Gopalswamy et al.*, 2000; *Zhang et al.*, 2003; *Xie et al.*, 2004; *Schwenn et al.*, 2005] can help to indicate whether a given CME-shock/ICME association is plausible or unlikely. We also take into consideration the solar source location implied by the CME/eruptive features. For example a central meridian source might be favored over a near-limb source, in particular if an ICME or magnetic cloud is involved in generating the storm. We should emphasize that the CME-ICME associations were considered by the working group members both individually (often using variations on the approach outlined above and taking into account additional information, such as energetic particle observations which may link solar events and interplanetary shocks) and collectively, to reduce the bias and thus improve the reliability of identification.

[22] We again use the storm on 27 July 2004 (Figure 2) as an example to illustrate the process of identifying the solar source. The solar wind speed at shock arrival is ~900 km/s. If we simply assume that the CME-driven shock travels from the Sun at this constant speed, a travel time of ~46 hour is implied, suggesting (since this is a "fast" event at 1 AU) an CME event after 0000 UT, 25 July as the source. Examining the LASCO CME catalog as well as the related images, there was only one halo CME in the search window, at 1454 UT on 25 July. This had a high projected speed (1333 km/s) which was consistent with the fast ICME seen at Earth allowing for some deceleration in the inner heliosphere. A direct association can also be demonstrated for this event using energetic particle observations which show an increase commencing at the time of the CME [*Cane et al.*, 2006] that reaches peak intensity in the vicinity of the passage of the ICME-driven shock. This CME was associated with a long duration M1.1 soft X-ray flare located at N04°W30°. The eruption at the surface was accompanied by a coronal dimming as shown in the running-difference EIT image (Figure 2g, middle). Both long duration flares and dimmings are well known surface manifestations of CMEs. This CME/flare originated in NOAA AR 0652 as indicated in the MDI magnetogram (Figure 2g, left).

[23] We should stress that it is not sufficient to use the time of the storm peak together with a plausible 1 AU transit time to estimate the time of the solar source. Rather, it is important to examine and characterize the solar wind structures within which the geoeffective region is embedded and then estimate the source timing. The effect of this distinction is illustrated by the event in Figure 2: the peak of the storm is ~16 hours after the arrival of the shock and ~12 hours after the arrival of the MC. These intervals are a significant fraction of the 1 AU transit times of the shock and ICME. Another point to note is that the two *Dst* minima in this storm result from two geoeffective regions, in the sheath and MC, associated with a single solar event. Such so called double-dip or two-step storms could be caused by a single ICME as well as multiple CMEs [*Kamide et al.*, 1998; *Farrugia et al.*, 2006].

3.3. Storms Involving Complex Solar Wind Structures and Multiple CMEs

[24] We classify the solar-IP drivers of the major geomagnetic storms into three broad categories: S-type, M-type, and C-type. S-type events are storms caused by single CMEs/ICMEs such as the 24 July 2004 storm described above. M-type are caused by multiple CMEs/ICMEs as discussed in this section. The C-type are for storms caused by CIRs [*Richardson et al.*, 2006]. For an M-type event, the storm is associated with complex solar wind structures that appear to involve multiple SHs and/or ICMEs. Two or more CMEs interact with each other in IP space, producing such complex flows [*Burlaga et al.*, 2002; *Zhang*

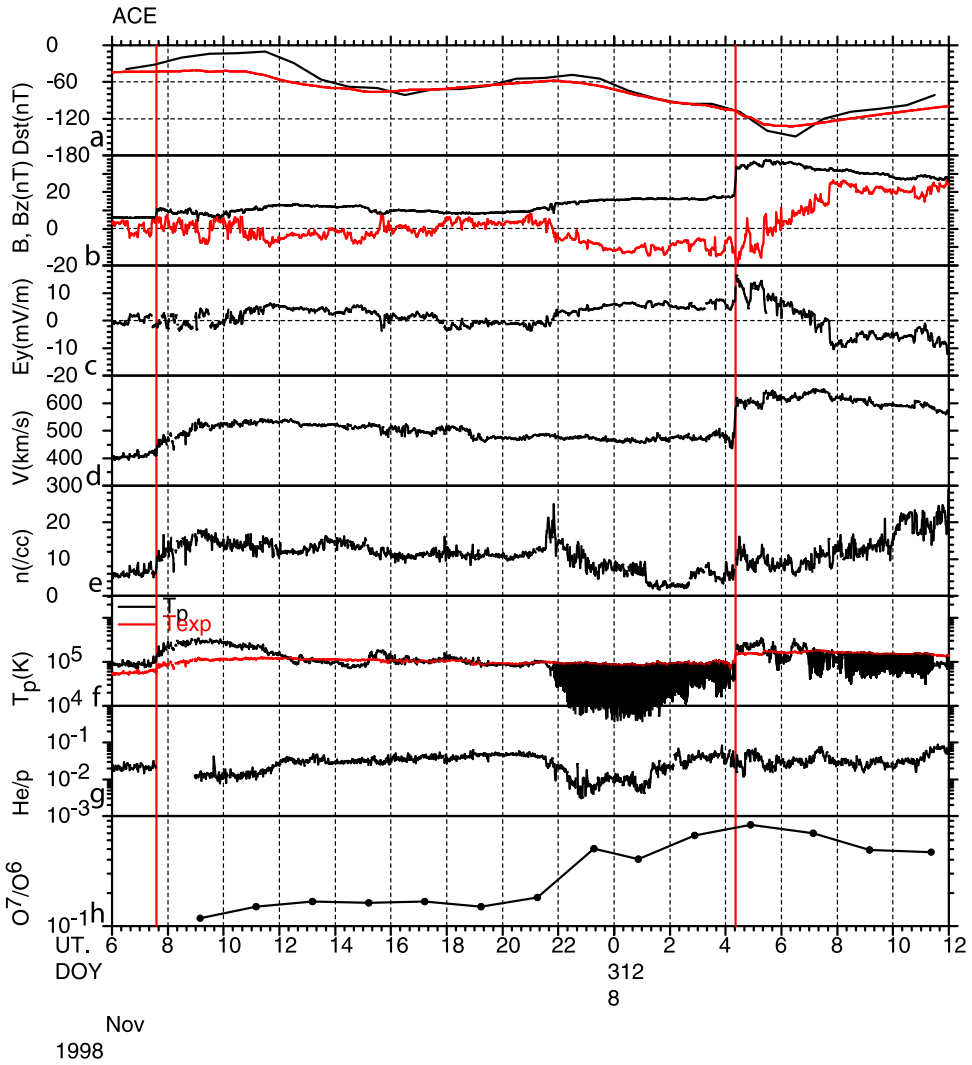

Figure 3. Geomagnetic and interplanetary data for the major geomagnetic storm (minimum *Dst* = −149 nT) on 8 November 1998 (event 16), showing, from top to bottom, (a) the observed *Dst* (black) with the predicted *Dst* index using the *O'Brien and McPherron* [2000] formula overlaid in red, (b) the magnetic field intensity (black) with B_z overlaid in red, (c) the Y-component of the solar wind electric field, (d) the solar wind velocity, (e) density, (f) proton temperature (black) and expected proton temperature (red) with the shaded black shading indicating where the proton temperature falls below the expected temperature, (g) helium/proton ratio, (h) and O^7/O^6 ratio. The two vertical red lines indicate the arrival times of ICME-driven shocks. Here, the peak of the storm is caused by an interplanetary shock (∼0400 UT on 8 November) propagating through a preceding ICME which has an embedded strong southward magnetic field.

et al., 2003; *Wang et al.*, 2003]. Direct observations of the interaction between two CMEs near the Sun have been reported [*Gopalswamy et al.*, 2001]. The M-type events are treated as a separate category from S-type because of the apparent differences in terms of the propagation/arrival of ICMEs, the resulting IP structures and geoeffective components.

[25] One interesting variety of M-type events that we have noted is when a storm is generated by a faster ICME-driven shock propagating into the trailing edge of a slower ICME that originated in an earlier event at the Sun. An example is the storm of 8 November 1998 (Event 16, minimum *Dst* = −149 nT) shown in Figure 3. This storm was clearly generated by the region of southward magnetic field between 2100 UT, 7 November, and 0500 UT, 8 November. The ACE plasma and field data show a weak shock at 0736 UT on 7 November followed by a probable ICME commencing at ∼2100 UT and indicated, for example, by the low proton temperature (black shading), enhanced magnetic field intensity, and enhancement in the solar wind O^7/O^6 ratio. The southward magnetic field in this structure generated the onset of the storm, reaching levels of *Dst* ∼ −100 nT. A second, stronger shock, propagating through the ICME passed ACE at 0421 UT on 8 November. The magnetic field in the first ICME was starting to turn toward the ecliptic at this time. However, the combination of the shock compression, which doubled the magnetic field strength and prevented the southward field strength from decaying, and

the increase in solar wind speed, enhanced the y-component of the solar wind electric field, thereby strengthening storm activity and producing the peak of the storm. We suggest that ICME-associated plasma forms the post-shock sheath, at least to the end of the interval shown. Note that the field here turned northward, causing *Dst* to decline rapidly after the storm peak. We associate the shock on 8 November with a 1119 km/s halo CME with a source at $N22°W18°$ on 5 November. Often in such situations, the source of the slower shock/ICME is less easily established. In the case of the shock on 7 November, however, we suggest that a 523 km/s halo CME at 0754 UT on 4 November originating from a quiet-Sun region associated with a quiescent filament is a likely candidate. We classify this storm as M-type because, although the arrival of the 8 November shock is clearly associated with the peak of the storm, the presence of the southward fields in the preceding ICME is also required to generate the storm.

[26] Before leaving this event, it is worth commenting on the chance juxtaposition of the 8 November shock, Earth and preceding ICME that generated the storm peak. Had the timing been slightly different, the storm peak strength could have been substantially different. For example, had the shock been delayed relative to the ICME by as little as an hour or so, it would have encountered a region of northward field. Hence the shock-ICME interaction would not have contributed to the storm. If the shock had arrived an hour or two earlier, it would have encountered stronger southward fields in the ICME, and an even more intense storm might have been generated. This clearly illustrates that while for S-type events involving one CME, there may be some hope in the future of predicting the geoeffectiveness using solar observations to infer the CME magnetic field structure, a similar prediction is far more difficult for M-type events.

4. Results and Discussions

4.1. Table of Solar and IP Sources

[27] On the basis of the methods described above, we have identified the solar and IP sources of the 88 major geomagnetic storms during 1996–2005. The results are summarized in Table 1. Columns 1 to 3 give the properties of each geomagnetic storm, as discussed earlier. In column 4, we list the overall solar-IP source type (S, M and C). Columns 5–10 describe the properties of solar source, and columns 11–14 the properties of the IP sources contributing to the geomagnetic activities. Column 15 indicates a (somewhat subjective) confidence level for our identifications, given as 1 to 3 in descending order of confidence. In the final column, ''F'' indicates that there are additional comments in a footnote. In many cases these summarize comments on the proposed associations, or alternative proposals, from working group members.

[28] Considering the properties of solar sources, the time in column 5 refers to the first appearance of the CME in the LASCO C2 coronagraph, the CME velocity in column 6 refers to the average speed of the CME through a linear fit in the LASCO C2/C3 fields of view, and the angular width in column 7 is the apparent angular span of the CME in the plane of the sky measured in the C2 field of view. These values were generally obtained from the on-line LASCO CME catalog. However, in a few cases, they refer to previously unlisted CMEs that were identified from a reexamination of the LASCO images. Column 8 shows the magnitude of the soft X-ray flare associated with the source CME. Column 9 shows the surface source region type, whether an ''AR'' (active region) followed by the four digit NOAA AR number, ''QS'' (quiet sun region), or ''CH'' (coronal hole). Note that quiet Sun regions here refer to any region on the surface of the Sun outside the traditional active regions and coronal holes. The sources of the CMEs from these regions are often associated with erupting quiescent filaments or filament channels.

[29] Column 10 gives the heliographic coordinates of the surface source region. This generally corresponds to the H_α flare location reported by NOAA SEC. When no H_α flare location is reported, we used EIT images to measure the source coordinates, given by the location of the compact brightening, if observed, or the centroid of the dimming region if no brightening was observed. If the surface source regions of the CME candidates are unknown due to the absence of any eruptive signature, this is indicated by ''UNK'' in columns 9 and 10. For events with LASCO/EIT data gaps, the solar sources could still be identified in some cases (events 6, 13, 14, and 21) if a major long-duration solar flare occurred at an appropriate time (based on consideration of transit times and in situ solar wind speeds, solar particle events, etc) and location. For these events, the time in column 5 is the flare onset time, followed by ''(F)'' to emphasize that this is not a CME time. Otherwise, ''DG'' in these columns indicates a gap in LASCO and/or EIT observations and that it is not possible to identify a probable source using alternative observations.

[30] In the case of M-type events, there are multiple rows for each event listing the multiple CMEs that may contribute to the observed 1 AU solar wind structures. In each case, the first row indicates what we suggest is the ''principal'' solar driver. In the case of C-type events, the definitions of the parameters in the solar source columns are slightly different because of the different nature of the source. The time in column 5 indicates the central meridian transit time of the centroid of the associated coronal hole measured from EIT images. The time is followed by ''(CH)'' in order to emphasize that this does not refer to a CME source. The heliographic coordinate in column 10 indicates the latitude of the coronal hole centroid when it crosses central meridian.

[31] Considering the properties of IP sources, column 11 characterizes the solar wind components that contribute to the storm, while columns 12, 13, and 14 show the time of the CME-driven shock (or disturbance, at either ACE, indicated by ''A,'' or WIND by ''W''), and the start and ending times of the ICME. In column 11, we indicate in bold typeface the specific component(s) that contain, and we believe, drives the peak of the geomagnetic storm. Normal type indicates that the structure contributes to enhanced geomagnetic activity, but only to levels of >-100 nT. A plus sign indicates a simple succession of components, while a dash indicates an ''interaction'' between the components. For example, for event 3, a sheath and magnetic cloud contribute to the geomagnetic activity. The sheath does not drive *Dst* to major storm levels, while the magnetic cloud includes the peak of the major storm. In contrast, for event 5, though the same structures are present,

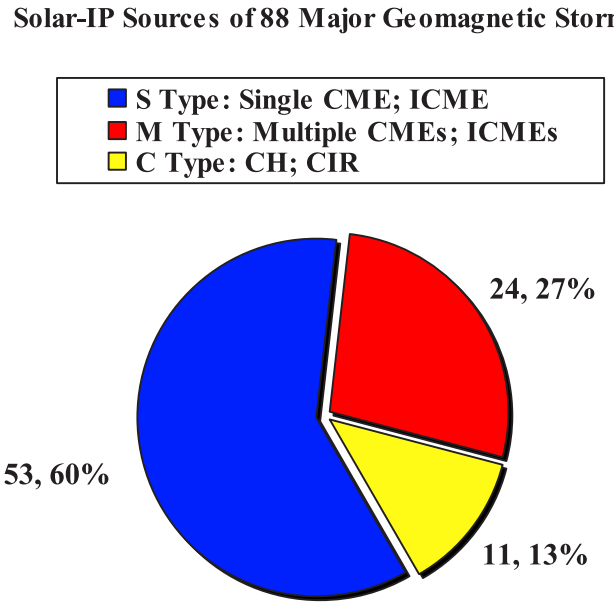

Figure 4. Distribution of the three types of solar-IP sources for the 88 major geomagnetic storms during 1996–2005.

the sheath drives the peak of the storm. For M-type events, it can be difficult to summarize in a compact way, or even to identify unambiguously, the various components present, but the nature of the specific components driving the storm is indicated, e.g., "SH(M)" means the presence of a sheath-like region that may include features (such as additional shocks) that suggest that more than one solar/interplanetary event contributes. The situation where a shock is running into a preceding ICME or magnetic cloud, as discussed earlier in relation to Figure 3 is indicated by PICME-SH or PMC-SH, respectively.

[32] Column 15 serves as an indicator of our group's confidence level of the identifications for each event. Levels 1, 2, and 3 indicate, with decreasing level of confidence, the most unambiguous, plausible, and ambiguous/uncertain identifications, respectively. For 47 (53%) of the storms would we regard our associations as level 1. These include most of the S-type and C-type events. The 27 (31%) level 2 storms include most M-type events and a few S-type. There are 14 (16%) events in level 3. Except several events that occurred during LASCO/EIT data gaps that gave rise to the uncertainty of identification, nine of the level 3 events (numbered as 2, 7, 28, 31, 34, 36, 40, 58, and 76 in Table 1) presented a perplexing situation. These nine events clearly showed ICME signatures in the solar wind observations. However, we were not able to find any conventional frontside halo CME candidates in the plausible search window, i.e., we fail to identify any eruptive feature on the solar surface (e.g., filament eruption, dimming, loop arcade, or long-duration flare), in spite of the availability of disk observations from EIT, SXT, or SXI. Similar "problem events" have been reported earlier [*Webb et al.*, 1998; *Zhang et al.*, 2003].

[33] Two possibilities might help to explain the problem events. First, as suggested by *Zhang et al.* [2003], an ICME may be caused by a very slow halo CME originating on the frontside of the Sun. Now we also think that it may be originated high in the corona, thus yielding no response in the low corona. This kind of halo CMEs may be mistakenly regarded as from the backside, due to the lack of obvious surface signatures. Indeed, we have been able to identify a slow halo CME that occurred 4 to 6 days before the arrival of the corresponding ICME for these problem events (except event 40); the transit time was generally consistent with that inferred from the observed CME and ICME speeds. We have reported such CMEs in Table 1. The second possibility is that an "unseen" CME, which exists but may not be seen by LASCO, causes an ICME. This could be due to the relatively poor "visibility" of a coronagraph when a CME is launched close to the disk center [e.g., *Yashiro et al.*, 2005]. For some problem events, we did find certain surface activities that might indicate an alternative driver; these activities were reported in the footnotes in Table 1. The above arguments may be consistent with the study of *Schwenn et al.* [2005], who reported that about 20% of ICMEs observed at the Earth, regardless of the intensity of the resulting geomagnetic activity, were not preceded by an identifiable frontside halo CME [see also *Cane and Richardson*, 2003]. In any case, we hope that more detailed analysis of data in the future may clarify the solar sources of at least some of these problem events.

4.2. On the Types of Overall Solar-IP Sources

[34] In Figure 4, we show the distribution of the three solar-IP source types for the 88 major geomagnetic storms during 1996–2005. The total numbers of S-type, M-type, and C-type events are 53 (60%), 24 (27%), and 11 (13%), respectively. Hence nearly two thirds of these major storms were generated by single events at the Sun and around another quarter involved multiple solar events. Considering S-type and M-type events together, we conclude that 77 (~87%) of the major storms in our study were driven by ICMEs (including the related upstream SHs) and hence originated from eruptive solar events, the remainder being associated with CIRs and hence with coronal holes. This result agrees with previous studies that have concluded that major geomagnetic storms are predominantly caused by ICMEs and their related structures [*Gosling et al.*, 1991; *Tsurutani et al.*, 1997; *Richardson et al.*, 2001].

[35] Nevertheless,, we also want to stress the nontrivial fraction (~13%) of these major geomagnetic storms that were driven by CIRs. A detailed analysis of the nine events from 1996–2004 has been reported by *Richardson et al.* [2006]. This is a somewhat surprising result but it is also a consequence of the −100 nT *Dst* storm threshold chosen for the workshops; the strongest CIR-associated storm had a *Dst* minimum of −131 nT so all these events would have been excluded had a lower *Dst* threshold been chosen. Furthermore, we note that three of the 88 major storms were generated by the interaction of a CIR with an ICME. These were events 22 (22 October 1999; $Dst = -237$ nT), event 58 (1 October 2002; $Dst = -176$ nT), and event 76 (30 August 2004; $Dst = -126$ nT). These three events have been classified as S-type in the table because it is the presence of the ICME that is critical to the generation of the storm.

[36] The year-by-year distribution of event types is shown in Figure 5. In 1996, the year of solar minimum, there was a single major storm driven by a CIR. Otherwise, during the

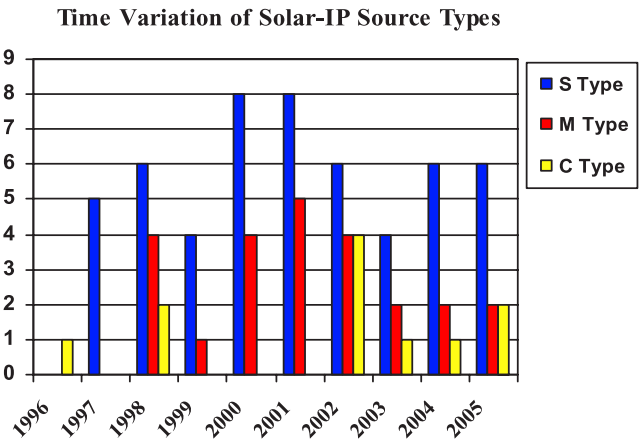

Figure 5. Solar cycle variation of the occurrence rate of the three types of solar-IP sources for the 88 major geomagnetic storms during 1996–2005.

rise, maximum, and declining phases of cycle 23, the major storms were predominantly driven by ICMEs with S-type dominating over M-type. C-type events were observed in 1996 and 1998, were absent during 1999–2001 around solar maximum even though low-latitude coronal holes and their associated streams were still typically present [*Luhmann et al.*, 2002], and reappeared in 2002 through 2005 during the declining phase of the cycle. The asymmetry in the number (three versus eight) of CIR-generated storms between the rising and declining phase of the cycle, with more during the declining phase, is typical of other studies [e.g., *Richardson et al.*, 2001]. Nevertheless, most major storms were still driven by ICMEs during 2002–2005.

[37] For the 77 CME-driven storm events, around two thirds (53; 69%) were S-type and one third (24; 31%) M-type. The ratio of the numbers of S and M-type events does not show any clear solar cycle variation. Although we might expect M-type events to be more prominent at higher solar activity levels because of the higher CME rate, M-type events occurred throughout the solar rising, maximum and declining phases, except in 1997, when all five events were S-type. S-type storms are still the most frequent type around solar maximum. The lack of a solar cycle dependence in the occurrence of M-type events may be due to the fact that for at least half of the 24 M-type storms, the responsible multiple CMEs originated from the same active region rather than from separate solar source regions. Such "super" active regions may appear at any phase of the solar cycle.

4.3. On Geoeffective Solar Wind Components

[38] Column 11 of Table 1 indicates that several configurations of IP structures gave rise to the major storms. For S-type events, the ICME and/or the upstream SH can contribute. We find that the storm peak was driven by the SH in 12 of these events (22%), by an ICME that is a magnetic cloud in 30 events (57%) and by a noncloud ICME in 11 events (21%). Hence a majority of major storms involving a single CME/ICME were driven to storm maximum by a magnetic cloud. For the M-type events, the IP drivers are typically more complex and involve multiple structures. Nevertheless, in most cases the storm driver can be characterized. In rare cases, such as event 10, a single driver among the various structures that pass the Earth (in this case a magnetic cloud) can be identified. A more common situation is that the storm peak is driven by a SH region or an ICME region that appears to include multiple components (indicated by SH(M) and ICME(M), respectively) that presumably reflect the complexity of the solar source. Multicomponent SH regions drive nine storms and multicomponent ICME or MC regions drive another six storms. The situation illustrated in Figure 3 in which a storm is caused by a shock propagating through a preceding ICME, drives the peak of nine M-type storms and hence is responsible for ~10% of all 88 major storms in this study.

[39] Considering the 53 S-type and 24 M-type CME-driven storms together, the geoeffective components are MCs in 33 events (43%), ICMEs without clear cloud signatures in 14 events (18%), SH regions in 21 events (27%), and, as noted above, shocks propagating through preceding ICMEs/MCs in nine events (12%). Hence consistent with other studies, MCs form the most important class of IP drivers of major geomagnetic storms [*Wu and Lepping*, 2002; *Huttunen et al.*, 2005]. This is despite the fact that only a minority of ICMEs at Earth, in particular around solar maximum, have magnetic cloud signatures [*Richardson and Cane*, 2004]. The reason is that the magnetic fields associated with magnetic clouds can, if correctly oriented, provide the extended intervals of strong southward fields that drive major storms, such as in Figure 2. Other ICMEs typically have less organized, more irregular magnetic fields that may also be less enhanced, and hence noncloud ICMEs are typically less geoeffective. Nevertheless, even if a magnetic cloud is present, it may not drive the peak of the storm if the cloud field orientation is not conducive for storm generation. For example, in event 5, it is the sheath ahead of the magnetic cloud that drives the peak of the storm. More than half of the major storms are associated with other structures which have less organized magnetic structure, and hence in principle have less "predictable" geomagnetic consequences [*Huttunen and Koskinen*, 2004].

4.4. On Solar CMEs Associated With Major Geomagnetic Storms

[40] Except for the ~10% of events driven by CIRs, all the other major geomagnetic storms in our survey were caused by IP transients following solar CMEs. After excluding events that occurred during LASCO data gaps, we were able to identify 68 CMEs that were the likely solar sources of these storms, as given in Table 1. Apparently, these 68 CMEs were the most effective in producing geomagnetic storms among thousands of CMEs observed during 1996–2005. When summarizing the properties of these CMEs, only the presumed "principle" CME (shown as the first CME in the list of possible multiple sources in the event table) was included for M-type events.

[41] Considering the apparent angular size of these CMEs, 46 (68%) were full halo CMEs and 22 (32%) were partial halo CMEs. Clearly, partial halo CMEs should be considered when searching for the solar drivers of major geomagnetic storms. During the same period, LASCO observed 1187 halo CMEs of which 378 (32%) were full halos and 809 (68%) were partial halos. Comparing with the

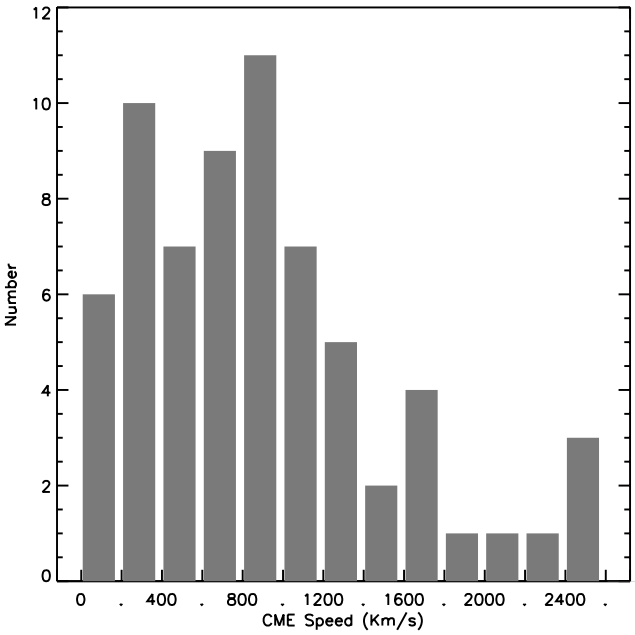

Figure 6. Distribution of the plane of the sky speeds for the 68 CMEs observed by SOHO/LASCO that resulted in major storms.

number of similar CMEs that produced major storms, we estimate that about one out of eight full halo CMEs (or one out of four frontside full halo CMEs, assuming that around half of halo CMEs originate on the backside of the Sun) will cause a major geomagnetic storm, and about 1 in 36 partial halo CMEs will do so. If all LASCO CMEs, 10,410 in total in the period of interest, are considered, on average only 1 out of ~150 CMEs will cause a major storm. Since halo CMEs comprise only a small fraction of all CMEs observed, it is practical to use these relatively rare events to predict the interception of an ICME by the Earth, and hence the possible generation of a geomagnetic storm. However, there is certainly not a one-to-one association between halo CMEs and ICMEs at Earth. About 15% of frontside halo CMEs may not intercept the Earth, and some 20% of ICMEs are not preceded by identifiable frontside halo CMEs [*Schwenn et al.*, 2005]. Furthermore, when an ICME does intercept the Earth, the magnetic field configuration still has to be conducive for the generation of a major storm. The ICME rate at Earth [*Cane and Richardson*, 2003], far exceeds the rate of major storms, for example by a factor of ~4 around solar maximum.

[42] In Figure 6 we display the speed distribution of the 68 CMEs associated with major geomagnetic storms. Remarkably, the distribution has a wide range from ~60 km/s to ~2800 km/s with evidence of a peak at about 900 km/s. The average (median) speed of the 68 CMEs is 945 km/s (875 km/s). A similar average speed (855 km/s) was obtained by *Gopalswamy* [2006] for a set of 55 geoeffective CMEs. For comparison, the average (median) speed of all 10410 CMEs in the study period is 472 km/s (410 km/s), and the average (median) speed of all 1187 halo CMEs is 767 km/s (636 km/s). The difference between the speeds of halo CMEs and the general population of CMEs is probably due to the relatively low detection rate of slow halo CMEs; a slow CME tends to be narrower and thus may fall below the LASCO detection threshold when it expands beyond the occulting disk as it has to propagate further from the Sun to become a visible halo [*Webb and Gopalswamy*, 2006]. The major storm-associated CMEs are on average around twice as fast as the all-CME average, in agreement with recent results [*Webb*, 2002; *Yashiro et al.*, 2004]. Forty-five (66%) of the 68 major storm-associated CMEs have speeds in the LASCO C2/C3 fields of view that exceed 600 km/s. These properties are consistent with the expectation that major geomagnetic storms are usually due to fast halo CMEs.

[43] Nevertheless, the relatively small difference (~200 km/s, compared with the breath of the distributions) between the average speeds for all halo CMEs and major storm-associated CMEs suggests that strongly geoeffective halo CMEs cannot necessarily be distinguished from other halo CMEs on the basis of their speed alone, as discussed earlier by *Zhang et al.* [2003]. Further, some very slow CMEs, though a small faction, can also generate major storms. Twelve (18%) of the 68 storm-associated CMEs had apparent speeds of less than 300 km/s. These results emphasize the fact that speed alone is not the major factor determining geoeffectiveness. Rather, the configuration of the embedded magnetic fields is also important, as exemplified by the fact that most of these storms associated with slow CMEs resulted from slow magnetic clouds at the Earth with speeds comparable to the ambient solar wind.

[44] Considering the association of major storms with GOES soft X-ray flares, we find that among the 77 CME-driven storms, 19 (25%) were associated with a X-class flare, 17 (22%) with a M-class flare, 19 (25%) with a C-class flare, and 22 (28%) with either minor (B or A-class), or with no evidence of a flare. We conclude that major (M or X-class) flares were associated with about one half of our major storms and that around a third of the storms were not accompanied by a flare or only by a minor flare. Therefore using flares, the traditional indicator of solar activity, to predict geomagnetic storms is often far from satisfactory [*Gosling*, 1993].

4.5. On the Solar Surface Source Regions Associated With Major Geomagnetic Storms

[45] Figure 7 summarizes nature of the solar surface source regions where the major storms in our study originated (Column 9 of Table 1). For three of the 88 events, there were insufficient data (e.g., data gap in LASCO/EIT observations, and no major flares reported in a plausible time window) for the source to be inferred. In the case of M-type events, we only include the source of the principle CME. We find that 54 storms (~63%) originated in active regions, 11 (13%) originated in quiet Sun regions, and 11 (13%) were associated with coronal holes. Here, quiet Sun region is a general reference to any coronal region other than active regions or coronal holes. It should be noted though that even when a CME originates outside an active region, it is usually associated with a quiescent filament or filament channel overlying a magnetic inversion line in the photosphere. For the remaining nine (11%) events we were unable to identify any solar surface signature and hence the nature of the source region is unknown. Thus while half of the major geomagnetic storms originated in active regions, a similar number originated outside active regions.

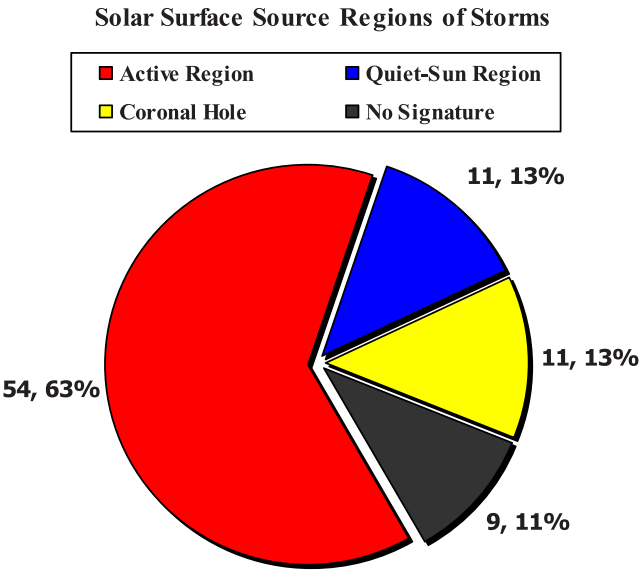

Figure 7. Types of solar surface source regions for the 88 major geomagnetic storms during 1996–2005.

[46] Nevertheless, active regions remain the source of the largest storms. The 10 largest storms (minimum Dst ≤ -271 nT) during 1996–2005 were all associated with active regions. For comparison, the largest storm that originated from a quiet Sun region reached $Dst = -237$ nT. Furthermore, the largest storm with an unknown surface source attained $Dst = -182$ nT, and the largest storm from a coronal hole source had a minimum Dst of only -131 nT.

[47] In Figure 8, we show the heliographic distribution of the source regions (Column 10 of Table 1). This distribution includes the 65 CMEs with identified surface sources. The other 23 events are excluded because they were associated with coronal holes (11 events), or unidentified sources (nine events), or occurred within solar data gaps (three events). The source locations lie within 35°N to 58°S latitude for active region (red symbols) and quiet Sun sources (blue symbols), and 61 of the 64 source regions (95%) lie within 30° from the equator. A possible explanation is that CMEs originating from higher latitudes propagate into the high-latitude region of the heliosphere and do not intercept the Earth.

[48] Considering the longitudinal distribution, 56 of the 65 source regions (86%) lie within 45° from central meridian, 49 (75%) within 30°, and 34 (52%) within 15°. Hence the vast majority of major storms arise from solar sources that are close to central meridian. The sources also show an east-west asymmetry that favors the western hemisphere and reinforces the similar result from the study of *Zhang et al.* [2003]. Specifically, the sources extend to 85°W, but only to 58°E, and 43 lie on the western hemisphere, compared with 20 on the eastern hemisphere (two events are at the central meridian). Hence the ratio of number of western to eastern sources is ~2:1. The average (median) longitude of all the 65 events studied is 12°W (8°W). Geoeffective CMEs could be from far western regions but not from far eastern regions. This east-west asymmetry seems to be a general feature of the ICMEs that intercept the Earth, regardless the strength of geoactivity [*Wang et al.*, 2002; *Cane and Richardson*, 2003]. One possible explanation is that this asymmetry results from the deflection of CME trajectories by the spiral IP magnetic field [*Wang et al.*, 2004].

4.6. Implication for Forecasting Major Geomagnetic Storms

[49] What are the implications of this study for forecasting major geomagnetic storms using solar observations? First, there may be a misconception that a major geomagnetic storm must be caused by an unusually fast halo CME from a strong active region accompanied by various energetic eruptive signatures (e.g., major solar flares). Except for the largest storms, this was not the case for many of the major storms ($Dst \leq -100$ nT). In fact, some of these storms were caused by moderate speed CMEs that may have originated outside of active regions, as well as by CIRs associated with coronal holes as described earlier. A central reason is that the driving electric field y-component depends on both the solar wind speed and B_s, but the variation of the size of B_s is greater than that of the solar wind speed. Furthermore, activity is suppressed when the IMF is northward, so a fast ICME with a predominantly strong northward field will not generate a major storm. The size of a storm also depends on the time variation of the southward field component. Thus a relatively slow moving MC with an extended region of enhanced southward field (such as event 15) can generate a major storm. Hence the speed of a halo CME alone is an inconsistent predictor of a major geomagnetic storm. Nevertheless, faster CMEs at the Sun are more likely to generate stronger storms because of their tendency to be associated with stronger magnetic field strengths and hence southward field components. It has been found that faster CMEs are statistically better correlated with parame-

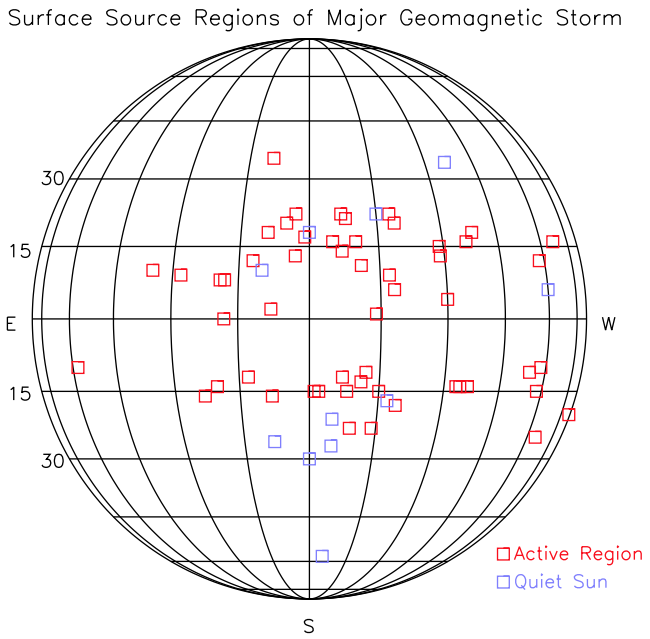

Figure 8. Heliographic locations of the 65 identified surface source regions for the CMEs that resulted in major geomagnetic storms during 1996–2005.

ters characterizing the geoeffectiveness [e.g., *Yurchyshyn et al.*, 2004; *Kim et al.*, 2005; *Moon et al.*, 2005]. A combination of CME speed and magnetic field in ICMEs seem to have a high correlation with Dst index [*Gopalswamy*, 2006]. A major advance would be to be able to "predict" the interplanetary magnetic field configuration at 1 AU, in particular for S-type storms involving only one CME/ICME, based on solar observations.

[50] In the case of storms that involve more than one CME/ICME, a complicating factor for forecasting is that it is the details of the magnetic structures formed by the interaction of these transients (and their associated shocks), both with each other and with the ambient solar wind, that determine the resulting level of geomagnetic activity. The precise path of the Earth through the structure is also a factor. Even with a relatively complete MHD simulation of two CMEs launched toward the Earth, it would be difficult to model the resulting fields at 1 AU on the necessary few-hour timescales. Information from upstream spacecraft would help to assess the likely geomagnetic impact, but the interacting structures may still evolve before reaching the Earth.

5. Summary

[51] We have investigated the solar and IP sources of the 88 major geomagnetic storms ($Dst \leq -100$ nT) that occurred during 1996–2005 with the aim of providing a list of associations that is as reliable as possible and is intended to provide a basis of future studies by the LWS CDAW participants and others. By combining remote-sensing solar observations, in situ near-Earth solar wind observations, and the wide range of experience of the Working Group members, we were able to identify with reasonable confidence the chain of sources for about 83% (73) of these events, although the detailed one-to-one association could not be established for those complex events involving multiple CMEs and ICMEs. We are uncertain of the origin of the other 17% (15) of the storms, mainly because their driving CMEs were not associated with noticeable eruption signatures at the solar surface. Detailed parameters of the solar and IP sources for each of the 88 major geomagnetic storms have been provided. The main results are as follows:

[52] 1. On the basis of the overall solar and IP properties, the sources can be divided into three broad categories: S-type, driven by single CMEs and their IP counterparts; M-type, associated with multiple CMEs/ICMEs, and C-type due to CIRs driven by high speed streams from coronal holes. The total numbers of S-type, M-type, and C-type events are 53 (60%), 24 (27%), and 11 (13%), respectively.

[53] 2. Of the 68 identified LASCO CMEs associated with major storms, 46 (68%) were full halo CMEs, and 22 (32%) were partial halo CMEs. Their speeds have a wide range (60 km/s to 2800 km/s). The average speed (945 km/s) is about twice as fast as the average for all LASCO CMEs. About half (47%) of these storm-associated CMEs were accompanied by major (X and M-class) flares.

[54] 3. For the 85 storms for which we could identify the solar surface source, we find that 54 ($\sim$63%) originated in active regions, 11 (13%) in quiet Sun regions associated with quiescent filaments, and 11 (13%) were associated with coronal holes. The other 9 (11%) events originated from unknown surface source regions.

[55] 4. Major geomagnetic storms predominantly originated from sources near central meridian (e.g., 86% from with 45°, and 75% from with 30° of central meridian) but showed an east-west asymmetry with around twice as many storm sources originating on the western hemisphere than on the eastern hemisphere.

[56] **Acknowledgments.** We acknowledge the many researchers who have contributed to the data used in this study. In particular, the ACE plasma, magnetic field, and composition/charge state data were provided by the ACE Science Center. SOHO is a project of international cooperation between ESA and NASA. The LASCO instrument was constructed by a consortium of the Naval Research Laboratory, University of Birmingham (England), the Max-Planck-Institute für Aeronomie (Germany), and the Laboratoire d'Astronomie Spatiale (France). We acknowledge the usage of the CME catalog generated and maintained at the CDAW Data Center by NASA and the Catholic University of America in cooperation with the Naval Research Laboratory. Travel support for some participants to the CDAW workshops is provided by NASA's LWS TR and T program. J. Z. acknowledges the support from NASA grants NNG04GN36G and NNG05GG19G and NSF SHINE grant ATM-0454612. D. F. W. acknowledges the support from AFRL contracts AF19628-00-C-0073 and FA8718-04-C-0050. N. V. N. acknowledges the support from NASA grant NNG05GK05G. A. N. Z. acknowledges the support from the Belgian Federal Science Policy Office through the ESA-PRODEX programme.

[57] Amitava Bhattacharjee thanks Yong-Jae Moon and another reviewer for their assistance in evaluating this paper.

References

Berdichevsky, D. B., C. J. Farrugia, B. J. Thompson, R. P. Lepping, D. V. Reames, M. L. Kaiser, J. T. Steinberg, S. P. Plunkett, and D. J. Michels (2002), Halo-coronal mass ejections near the 23rd solar minimum: Lift-off, inner heliosphere, and in situ (1 AU) signatures, *Ann. Geophys.*, *20*, 891–916.

Brueckner, G. E., et al. (1995), The large angle spectroscopic coronagraph (LASCO), *Sol. Phys.*, *162*, 357–402.

Brueckner, G. E., J.-P. Delaboudiniere, R. A. Howard, S. E. Paswaters, O. C. St. Cyr, R. Schwenn, P. Lamy, G. M. Simnett, B. Thompson, and D. Wang (1998), Geomagnetic storms caused by coronal mass ejections (CMEs): March 1996 through June 1997, *Geophys. Res. Lett.*, *25*, 3019–3022.

Burlaga, L. F., S. P. Plunkett, and O. C. St. Cyr. (2002), Successive CMEs and complex ejecta, *J. Geophys. Res.*, *107*(A10), 1266, doi:10.1029/2001JA000255.

Cane, H. V., and I. G. Richardson (2003), Interplanetary coronal mass ejections in the near-Earth solar wind during 1996–2002, *J. Geophys. Res.*, *108*(A4), 1156, doi:10.1029/2002JA009817.

Cane, H. V., I. G. Richardson, and O. C. St. Cyr. (2000), Coronal mass ejections, interplanetary ejecta and geomagnetic storms, *Geophys. Res. Lett.*, *27*, 3591–3594.

Cane, H. V., R. A. Mewaldt, C. M. S. Cohen, and T. T. von Rosenvinge (2006), Role of flares and shocks in determining solar energetic particle abundances, *J. Geophys. Res.*, *111*, A06S90, doi:10.1029/2005JA011071.

Cliver, E. W., Y. Kamide, and A. G. Ling (2002), The semiannual variation of geomagnetic activity: Phases and profiles for 130 years of aa data, *J. Atmos. Terr. Phys.*, *64*, 47–53.

Crooker, N. U., E. W. Cliver, and B. T. Tsurutani (1992), The semiannual variation of great geomagnetic storms and the postshock Russell-Mcpherron effect preceding coronal mass ejecta, *Geophys. Res. Lett.*, *19*, 429–432.

dal Lago, A., et al. (2004), Great geomagnetic storms in the rise and maximum of solar cycle 23, *Braz. J. Phys.*, *34*, 1542–1546.

Delaboudiniere, J.-P., et al. (1995), EIT: Extreme-ultraviolet imaging telescope for the SOHO mission, *Sol. Phys.*, *162*, 291–312.

Dungey, J. R. (1961), Interplanetary magnetic field and auroral zones, *Phys. Rev. Lett.*, *6*, 47–48.

Farrugia, C. J., V. K. Jordanova, M. F. Thomsen, G. Lu, S. W. H. Cowley, and K. W. Ogilvie (2006), A two-ejecta event associated with a two-step geomagnetic storm, *J. Geophys. Res.*, *111*, A11104, doi:10.1029/2006JA011893.

Forsyth, R. J., and E. Marsch (1999), Solar origin and interplanetary evolution of stream interfaces, *Space Sci. Rev.*, *89*, 7–20.

Gonzalez, A. L., V. M. Silbergleit, W. D. Gonzalez, and B. T. Tsurutani (2002), Irregularities in the semiannual variation of the geomagnetic activity, *Adv. Space Res.*, *30*, 2215–2218.

Gonzalez, W. D., J. A. Joselyn, Y. Kamide, H. W. Kroehl, G. Rostoker, B. T. Tsurutani, and V. M. Vasyliünas (1994), What is a geomagnetic storm?, *J. Geophys. Res.*, *99*, 5771–5792.

Gopalswamy, N. (2006), Coronal mass ejections of solar cycle 23, *J. Astrophys. Astron.*, *27*, 243–254.

Gopalswamy, N., A. Lara, R. P. Lepping, M. L. Kaiser, D. Berdichevsky, and O. C. St. Cyr. (2000), Interplanetary acceleration of coronal mass ejections, *Geophys. Res. Lett.*, *27*, 145–148.

Gopalswamy, N., S. Yashiro, M. L. Kaiser, R. A. Howard, and J. L. Bougeret (2001), Radio signatures of coronal mass ejection interaction: Coronal mass ejection cannibalism?, *Astrophys. J.*, *548*, L91–L94.

Gopalswamy, N., S. Yashiro, G. Michalek, H. Xie, R. P. Lepping, and R. A. Howard (2005), Solar source of the largest geomagnetic storm of cycle 23, *Geophys. Res. Lett.*, *32*, L12S09, doi:10.1029/2004GL021639.

Gosling, J. T. (1993), The solar flare myth, *J. Geophys. Res.*, *98*(A11), 18,937–18,950.

Gosling, J. T., and D. J. McComas (1987), Field line draping about fast coronal mass ejecta—A source of strong out-of-the-ecliptic interplanetary magnetic fields, *Geophys. Res. Lett.*, *14*, 355–358.

Gosling, J. T., D. J. McComas, J. L. Phillips, and S. J. Bame (1991), Geomagnetic activity associated with Earth passage of interplanetary shock disturbances and coronal mass ejections, *J. Geophys. Res.*, *96*, 7831–7839.

Hill, S. M., et al. (2005), The NOAA Goes-12 Solar X-Ray Imager (SXI): 1. Instrument, operations, and data, *Sol. Phys.*, *226*, 255–281.

Howard, R. A., D. J. Michels, N. R. Sheeley Jr., and M. J. Koomen (1982), The observation of a coronal transient directed at Earth, *Astrophys. J.*, *263*, L101–L104.

Huttunen, K., and H. Koskinen (2004), Importance of post-shock streams and sheath region as drivers of intense magnetospheric storms and high-latitude activity, *Ann. Geophys.*, *22*, 1729–1738.

Huttunen, K. E. J., R. Schwenn, V. Bothmer, and H. E. J. Koskinen (2005), Properties and geoeffectiveness of magnetic clouds in the rising, maximum and early declining phases of solar cycle 23, *Ann. Geophys.*, *23*, 625–641.

Jackson, B. V., et al. (2004), The Solar Mass-Ejection Imager (SMEI) mission, *Sol. Phys.*, *225*, 177–207.

Kamide, Y., N. Yokoyama, W. Gonzalez, B. T. Tsurutani, I. A. Daglis, A. Brekke, and S. Masuda (1998), Two-step development of geomagnetic storms, *J. Geophys. Res.*, *103*, 6917–6922.

Kim, R.-S., K.-S. Cho, Y.-J. Moon, Y.-H. Kim, Y. Yi, M. Dryer, S.-C. Bong, and Y.-D. Park (2005), Forecast evaluation of the coronal mass ejection (CME) geoeffectiveness using halo CMEs from 1997 to 2003, *J. Geophys. Res.*, *110*, A11104, doi:10.1029/2005JA011218.

Klein, L. W., and L. F. Burlaga (1982), Interplanetary magnetic clouds at 1 AU, *J. Geophys. Res.*, *87*, 613–624.

Krall, J., V. B. Yurchyshyn, S. Slinker, R. M. Skoug, and J. Chen (2006), Flux rope model of the 2003 October 28–30 coronal mass ejection and interplanetary coronal mass ejection, *Astrophys. J.*, *642*, 541–553.

Lepping, R. P., C.-C. Wu, and D. B. Berdichevsky (2005), Automatic identification of magnetic clouds and cloud-like regions at 1 AU: Occurrence rate and other properties, *Ann. Geophys.*, *23*, 2687–2704.

Lepri, S. T., T. H. Zurbuchen, L. A. Fisk, I. G. Richardson, H. V. Cane, and G. Gloeckler (2001), Iron charge distribution as an identifier of interplanetary coronal mass ejections, *J. Geophys. Res.*, *106*, 29,231–29,238.

Lindsay, G. M., J. G. Luhmann, C. T. Russell, and J. T. Gosling (1999), Relationships between coronal mass ejection speeds from coronagraph images and interplanetary characteristics of associated interplanetary coronal mass ejections, *J. Geophys. Res.*, *104*, 12,515–12,524.

Luhmann, J. G., Y. Li, C. N. Arge, P. R. Gazis, and R. Ulrich (2002), Solar cycle changes in coronal holes and space weather cycles, *J. Geophys. Res.*, *107*(A8), 1154, doi:10.1029/2001JA007550.

Moon, Y.-J., K.-S. Cho, M. Dryer, Y.-H. Kim, S.-C. Bong, J. Chae, and Y. D. Park (2005), New geoeffective parameters of very fast halo coronal mass ejections, *Astrophys. J.*, *624*, 414–419.

Neugebauer, M., and R. Goldstein (1997), Particle and field signatures of coronal mass ejections in the solar wind, in *Coronal Mass Ejections*, *Geophys. Monogr. Ser.*, vol. 99, edited by N. Crooker, J. A. Joselyn, and J. Feynman, pp. 245–251, AGU, Washington, D. C.

O'Brien, T. P., and R. L. McPherron (2000), An empirical phase space analysis of ring current dynamics: Solar wind control of injection and decay, *J. Geophys. Res.*, *105*, 7707–7719.

Perreault, P., and S.-I. Akasofu (1978), A study of geomagnetic storms, *Geophys. J.*, *54*, 547–573.

Richardson, I. G., and H. V. Cane (1995), Regions of abnormally low proton temperature in the solar wind (1965–1991) and their association with ejecta, *J. Geophys. Res.*, *100*, 23,397–23,412.

Richardson, I. G., and H. V. Cane (2004), The fraction of interplanetary coronal mass ejections that are magnetic clouds: Evidence for a solar cycle variation, *Geophys. Res. Lett.*, *31*, L18804, doi:10.1029/2004GL020958.

Richardson, I. G., E. W. Cliver, and H. V. Cane (2001), Sources of geomagnetic storms for solar minimum and maximum conditions during 1972–2000, *Geophys. Res. Lett.*, *28*, 2569–2572.

Richardson, I. G., H. V. Cane, and E. W. Cliver (2002), Sources of geomagnetic activity during nearly three solar cycles (1972–2000), *J. Geophys. Res.*, *107*(A8), 1187, doi:10.1029/2001JA000504.

Richardson, I. G., et al. (2006), Major geomagnetic storms (Dst ≤ -100 nT) generated by corotating interaction regions, *J. Geophys. Res.*, *111*, A07S09, doi:10.1029/2005JA011476.

Russell, C. T., and R. L. McPherron (1973), Semiannual variation of geomagnetic activities, *J. Geophys. Res.*, *78*, 92–108.

Scherrer, P. H., et al. (1995), The Solar Oscillations Investigation—Michelson Doppler imager, *Sol. Phys.*, *162*, 129–188.

Schwenn, R., A. Dal Lago, E. Huttunen, and W. D. Gonzalez (2005), The association of coronal mass ejections with their effects near the Earth, *Ann. Geophys.*, *23*, 1033–1059.

Thompson, B. J., S. P. Plunkett, J. B. Gurman, J. S. Newmark, O. C. St. Cyr, and D. J. Michels (1998), SOHO/EIT observations of an Earth-directed coronal mass ejection on May 12, 1997, *Geophys. Res. Lett.*, *25*, 2465–2468.

Tsuneta, S., L. Acton, M. Bruner, J. Lemen, W. Brown, R. Caravalho, R. Catura, S. Freeland, B. Jurcevich, and J. Owens (1991), The soft X-ray telescope for the SOLAR-A mission, *Sol. Phys.*, *136*, 37–67.

Tsurutani, B. T., and W. D. Gonzalez (1997), The interplanetary causes of magnetic storms: A review, in *Magnetic Storms*, *Geophys. Monogr. Ser.*, vol. 98, edited by B. T. Tsurutani et al., pp. 77–89, AGU, Washington, D. C.

Tsurutani, B. T., W. D. Gonzalez, Y. Kamide, and J. K. Arballo (Eds.) (1997), *Magnetic Storms*, *Geophys. Monogr. Ser.*, vol. 98, AGU, Washington, D. C.

Tsurutani, B. T., et al. (2006a), Corotating solar wind streams and recurrent geomagnetic activity: A review, *J. Geophys. Res.*, *111*, A07S01, doi:10.1029/2005JA011273.

Tsurutani, B., R. McPherron, W. Gonzalez, G. Lu, J. Sobral, and N. Gopalswamy (2006b), *Recurrent Magnetic Storms: Corotating Solar Wind Streams*, *Geophys. Monogr. Ser.*, vol. 167, AGU, Washington, D. C.

Wang, Y. M., P. Z. Ye, S. Wang, G. P. Zhou, and J. X. Wang (2002), A statistical study on the geoeffectiveness of Earth-directed coronal mass ejections from March 1997 to December 2000, *J. Geophys. Res.*, *107*(A11), 1340, doi:10.1029/2002JA009244.

Wang, Y. M., P. Z. Ye, and S. Wang (2003), Multiple magnetic clouds: Several examples during March–April, 2001, *J. Geophys. Res.*, *108*(A10), 1370, doi:10.1029/2003JA009850.

Wang, Y., C. Shen, P. Ye, and S. Wang (2004), Deflection of coronal mass ejection in the interplanetary medium, *Sol. Phys.*, *222*, 329–343.

Webb, D. F. (2002), CMEs and the solar cycle variation in their geoeffectiveness, in *From Solar Min to Max: Half a Solar Cycle with SOHO*, edited by A. Wilson, *Eur. Space Agency Spec. Publ.*, *ESA SP-508*, 409–419.

Webb, D. F., and N. Gopalswamy (2006), Coronal mass ejections and space weather, in *Proceedings of the ILWS Workshop*, edited by N. Gopalswamy and A. Bhattacharyya, pp. 71–80, Quest, Denver, Colo.

Webb, D. F., E. W. Cliver, N. Gopalswamy, H. S. Hudson, and O. C. St. Cyr (1998), The solar origin of the January 1997 coronal mass ejection, magnetic cloud and geomagnetic storm, *Geophys. Res. Lett.*, *25*, 2469–2472.

Webb, D. F., E. W. Cliver, N. U. Crooker, O. C. St. Cyr., and B. J. Thompson (2000), Relationship of halo coronal mass ejections, magnetic clouds, and magnetic storms, *J. Geophys. Res.*, *105*, 7491–7508.

Webb, D. F., N. U. Crooker, S. P. Plunkett, and O. C. St. Cyr (2001), The solar sources of geoeffective structures, in *Space Weather*, *Geophys. Monogr. Ser.*, vol. 125, edited by S. Paul, J. S. Howard, and L. S. George, pp. 123–142, AGU, Washington, D. C.

Webb, D. F., et al. (2006), Solar Mass Ejection Imager (SMEI) observations of coronal mass ejections (CMEs) in the heliosphere, *J. Geophys. Res.*, *111*, A12101, doi:10.1029/2006JA011655.

Wimmer-Schweingruber, R. F., et al. (2006), Understanding interplanetary coronal mass ejection signatures, *Space Sci. Rev.*, *123*, 177–216.

Wu, C.-C., and R. P. Lepping (2002), Effects of magnetic clouds on the occurrence of geomagnetic storms: The first 4 years of Wind, *J. Geophys. Res.*, *107*(A10), 1314, doi:10.1029/2001JA000161.

Xie, H., L. Ofman, and G. Lawrence (2004), Cone model for halo CMEs: Application to space weather forecasting, *J. Geophys. Res.*, *109*, A03109, doi:10.1029/2003JA010226.

Yashiro, S., N. Gopalswamy, G. Michalek, O. C. St. Cyr, S. P. Plunkett, N. B. Rich, and R. A. Howard (2004), A catalog of white light coronal mass ejections observed by the SOHO spacecraft, *J. Geophys. Res.*, *109*, A07105, doi:10.1029/2003JA010282.

Yashiro, S., N. Gopalswamy, S. Akiyama, G. Michalek, and R. A. Howard (2005), Visibility of coronal mass ejections as a function of flare location and intensity, *J. Geophys. Res.*, *110*, A12S05, doi:10.1029/2005JA011151.

Yurchyshyn, V., H. Wang, and V. Abramenko (2004), Correlation between speeds of coronal mass ejections and the intensity of geomagnetic storms, *Space Weather*, *2*, S02001, doi:10.1029/2003SW000020.

Yurchyshyn, V., C. Liu, V. Abramenko, and J. Krall (2006), The May 13, 2005 eruption: Observations, data analysis and interpretation, *Sol. Phys.*, *239*, 317–335.

Zhang, J., K. P. Dere, R. A. Howard, and V. Bothmer (2003), Identification of solar sources of major geomagnetic storms between 1996 and 2000, *Astrophys. J.*, *582*, 520–533.

Zurbuchen, T. H., and I. G. Richardson (2006), In-situ solar wind and magnetic field signatures of interplanetary coronal mass ejections, *Space Sci. Rev.*, *123*, 31–43.

N. Gopalswamy and S. Yashiro, Solar System Exploration, NASA Goddard Space Flight Center, Code 695, Greenbelt, MD 20771, USA. (gopals@ssedmail.gsfc.nasa.gov; yashiro@ssedmail.gsfc.nasa.gov)

E. Huttunen, Space Sciences Laboratory, University of California, Berkeley, 7 Gauss Way 7450, Berkeley, CA 94720-7450, USA. (huttunen@ssl.berkeley.edu)

J. C. Kasper, Kavli Institute for Astrophysics and Space Research, Massachusetts Institute of Technology, 77 Massachusetts Avenue, Cambridge, MA 02139, USA. (jck@mit.edu)

N. V. Nitta, Lockheed Martin Solar and Astrophysics Laboratory, B/252, Dept/ADBS, 3251 Hanover Street, Palo Alto, CA 94304, USA. (nitta@lmsal.com)

W. Poomvises and J. Zhang, Department of Computational and Data Sciences, George Mason University, 4400 University Drive, MSN 6A2, Fairfax, VA 22030, USA. (wpoomvis@gmu.edu; jzhang7@gmu.edu)

I. G. Richardson, NASA Goddard Space Flight Center, Code 661, Greenbelt, MD 20771, USA. (ian.richardson@gsfc.nasa.gov)

B. J. Thompson, NASA Goddard Space Flight Center, Code 612, Greenbelt, MD 20771, USA. (barbara.j.thompson@nasa.gov)

D. F. Webb, Institute for Scientific Research, Boston College, 140 Commonwealth Avenue, Chestnut Hill, MA 02467, USA. (david.webb.ctr@hanscom.af.mil)

C.-C. Wu, NASA Goddard Space Flight Center, Code 696, Greenbelt, MD 20771, USA. (wuc@cspar.uah.edu)

A. N. Zhukov, Royal Observatory of Belgium, Avenue Circulaire 3, B-1180 Brussels, Belgium. (andrei.zhukov@oma.be)